Università degli Studi di Genova

Facoltà di Scienze Matematiche Fisiche e Naturali

Dipartimento di Chimica e Chimica Industriale

Ph.D. Thesis

Reactivity under cover in controlled Near Ambient Pressure conditions: CO on bare and graphene covered Ni(111)

Rocco Davì

Suoervisors: Prof. Mario Rocca (Università di Genova, Italy)

Dott.ssa Letizia Savio (CNR-IMEM, Italy)

Referees: Prof. Giovanni Comelli (Università di Trieste, Italy)

Prof. Rocco Martinazzo (Università Statale di Milano, Italy)

Genova March 6th 2021

Table of Contents

1. Abstract

The graphene–metal interface, as an interesting graphene-based system, attracts much attention from both the application and the fundamental science points of view. One of the reasons is that Chemical Vapor Deposition (CVD) on metal surfaces is the most promising method to produce large area graphene sheets with nickel and copper as most frequently used substrates. However, Ni has a severe drawback due to the high solubility of carbon at the temperatures required for CVD (>800 K). Dissolved carbon atoms may segregate to the surface of the substrate while cooling down the system, producing unwanted graphene multilayer structures. Careful preparation protocols have therefore to be followed, which leave carbide traces on the surface which can absorb the segregating carbon atoms by transforming into graphene. Another reason is that the graphene properties may be strongly affected by the interaction with the substrate, thus yielding interesting catalytic properties. My thesis is focused on the interaction of CO with Ni(111) which I studied in operando conditions with Near Ambient Pressure by X-Ray Photoemission Spectroscopy (NAP-XPS) at ~ 3 mbar thus extending the so far explored pressure range by nearly one order of magnitude. Under these conditions I observed the detachment of the strongly interacting graphene and its conversion into weakly interacting graphene caused by CO intercalation under it already at 500 K. Intercalation of gases is important since it restores the Dirac cone and thus the exceptionally large carrier mobility of graphene and because chemical reactions may be favored under cover by the constrained volume. Indeed, above 600 K, formation of physisorbed CO_2 is observed under the graphene cover, a process I ascribe to the onset of the Boudouard reaction. The latter leads to the formation of additional carbon atoms which transform the residual carbide, present at the surface, into graphene causing the expansion of the graphene islands. Furthermore, my data confirm that CO does not only intercalate, but adsorbs also above the strongly interacting graphene areas forming a weakly bonded species of possible catalytical relevance. The reaction has been observed also after drilling single and double vacancies into the graphene layer by ion bombardment. CO_2 tends then to mend the vacancies forming a bridge over their borders.

2. Introduction

Graphene state of art

Graphene (G) is a carbon allotrope consisting of a single-atom-thick sheet of carbon atoms arranged on a honeycomb lattice and bound together by strong sp^2 bonds. It forms readily on metal surfaces, but its relevance was disclosed only in 2004 by A. K. Geim and A. Novoselov (Novoselov 2005), who firstly reported on the wonderful properties dictated by its 2-dimensional nature. Indeed, graphene shows unique properties that make it very interesting for fundamental research and extremely promising for technological applications.

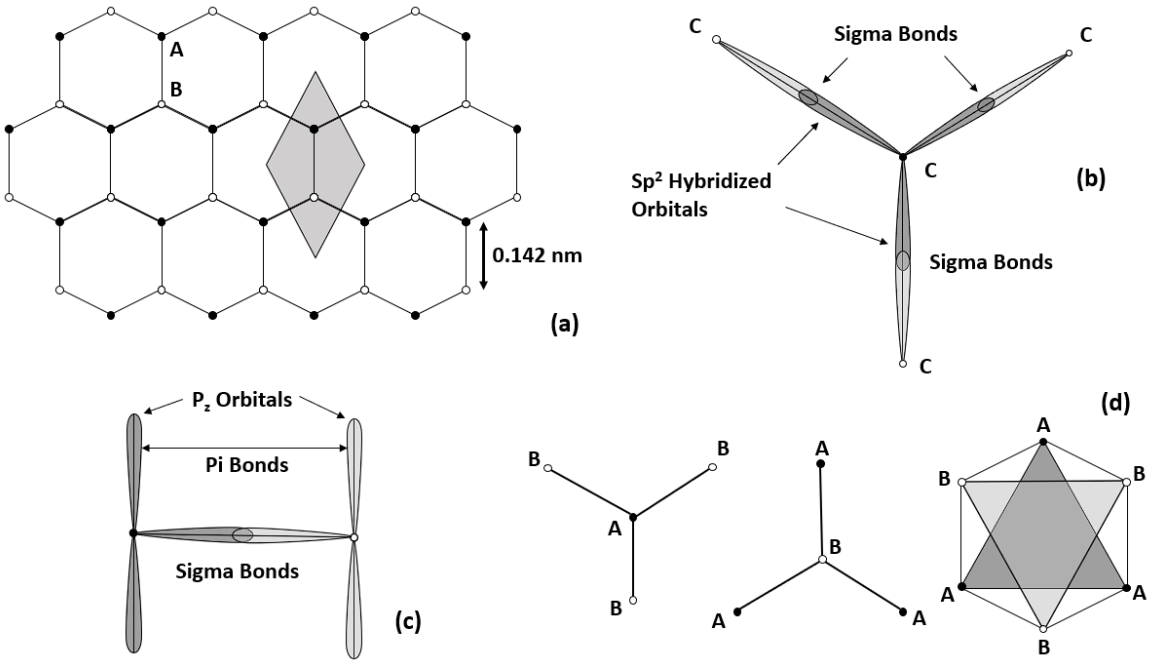

Figure 1 - Graphene lattice structure: a) honeycomb arrangement of carbon atoms, the unit cell (grey) contains two atoms A (black) and B (white) which sit 0.142 nm apart. (b) sp^2 hybridized orbitals forming three σ-bonds with the three nearest neighbors in the plane. (c) π bonds are formed by the p_z orbitals. (d) The figure highlights the different environment of atoms in A and B lattice sites.

The Graphene structure is show in figure 1. The lattice exhibits hexagonal symmetry and belongs to the P6/mmm space group with two inequivalent C atoms in the unit cell sitting at A and B sites respectively, which are 0.142 nm, apart (at least in the pristine graphene configuration). The carbon atoms are bonded together by σ-bonds arising from the overlap of the sp^2 hybridized orbitals. The remaining electrons occupy the p_z orbitals which form π-bonds.

The G band structure is characterized by linearly dispersing states near the Fermi Edge, forming cones in the band structure near the K and K' points (Dirac Cones). Because of this G is a zero-bandgap semiconductor (also addressed as semi-metal in older books) and can be easily

transformed into a semiconductor by adsorption of gases or by the interaction with a substrate. The linear dispersion implies an exceptionally high electron mobility since the effective mass of the charge carriers vanishes (even if the cyclotron mass of the carriers is non-zero - but as low as 0.02 m_e (Novoselov 2005)). Initially, applications were therefore envisaged to concern mainly nanoelectronics.

More recently, researchers started to investigate also other possible applications for graphene, in particular the possibility to employ it in nano sensor devices and as catalyst. In these perspectives, it could reduce the need for rare or expensive materials or eventually replace them altogether. The high surface/volume ratio of G implies that a huge surface area can be obtained from a very tiny quantity of carbon, which is anyhow a cheap and common material. Nonetheless, the price of G is presently mainly determined by its production cost, which is rapidly decreasing thanks to the large efforts devoted to the optimization of the production techniques. A further substantial decrease in the cost is expected when the production methods will scale up to mass production.

More and more methods for a massive production have been developed and engineered, but all of them can be roughly classified into two main groups: mechanical exfoliation of graphite and epitaxial growth on metal or semiconductor surfaces.

To the first category belongs the scotch tape method originally used by Geim and Novoselov, which still is the most widely employed to produce relatively large area flakes with optimal electronic properties to be used in transport experiments.

Production through sonication of high purity graphite crystals can also be envisaged: this method allows to produce graphene in large amount but the flakes are usually smaller (up to a few 100 nm), less pure and mostly oxidized. A reduction process is then needed to obtain pure graphene, but efficient production without degrading the quality of the graphene layer remains a challenge.

The second group of production processes consists in epitaxial growth methods, including Chemical Vapour Deposition (CVD), Molecular Beam Epitaxy (MBE) and growth by surface segregation. All these processes are usually applied to grow large area and high-quality graphene layers on transition metals surfaces but also on other materials like Silicon Carbide (SiC). The quality of the grown film depends on the choice of the substrate and varies widely. With it also the electronic and mechanical properties can be tailored.

A wide range of transition metals can be used to grow graphene by CVD, either in pure state (Ru, Pt, Ir, Rh, Co, Ni or Cu) or in alloys (Au-Ni, Cu-Ni, Ni-Mo). Most of the research has been focused on Ni and Cu as representatives of substrates with opposite behaviour.

The different strength of the substrate-film interaction manifests itself in the larger or weaker deformation of the graphene bands. As reported in the lower the adsorption distance, the higher is the interaction and the larger the band structure deformation.

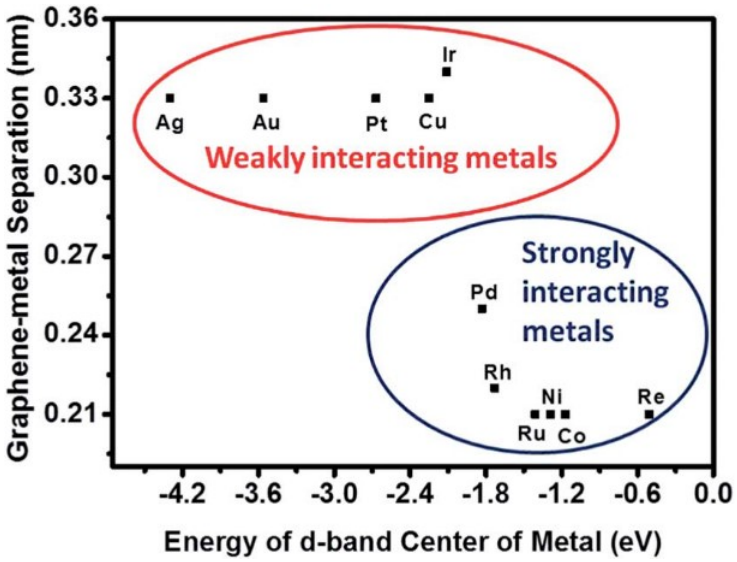

Figure 2 - Illustration of the correlation of graphene/metal separation with the energy of the d-band centre position (approx. 2eV below Fermi level). Taken from (Dahal 2014).

Ni and Cu have a quite different degree of interaction with the G layer: while Cu is a prototypical weakly interacting metal substrate with a metal-G separation of about 3.3 Å, Ni is strongly interacting, and the adsorption distance shortens to 2.1 Å. As a comparison, the interlayer separation of graphene planes in graphite is 3.35 Å. In general, growth on strongly interacting substrates, such as Ni, requires lower substrate temperature and lower pressure of the precursor hydrocarbon used in CVD than weakly interacting substrates, such as Cu.

An alternative growth method takes advantage of carbon dissolved into the bulk of the substrate. For most bulk metals, dissolved carbon can be driven to the surface by thermal annealing, a phenomenon known as segregation. This carbon can be used as a source for graphene production, as demonstrated for Ni, Co, Fe and Cu-Ni polycrystalline films (Liu et al. 2011).

The mechanism of graphene growth by carbon segregation proceeds in three steps:

1) thermally induced diffusion of dissolved carbon to the surface;
2) creation of growth-nuclei by trapping carbon atoms at grain boundaries and at step edges;
3) graphene growth around those centers when the temperature is lowered.

Graphene production via segregation easily yields multilayer graphene, in contrast to the single layer limitation of the CVD method. It is particularly efficient on Ni, Co and Pd due to their high carbon solubility (2.03%, 3.41% and 8.98% respectively), while it is strongly suppressed on metals having very low maximum carbon solubility, like Cu (0.04%) (Dahal 2014).

In experiments the carbon content of the sample is firstly increased by exposure to ethene at very high temperatures, then the hydrocarbon source is closed, and the substrate is slowly cooled down to promote graphene nucleation by segregation.

Chemical Vapor Deposition (CVD) relies on the catalytic decomposition of hydrocarbons on hot metal surfaces. The mechanism of graphene growth by CVD involves:

1) decomposition at the substrate surface;
2) graphene nucleation;
3) expansion of the graphene island size.

CVD growth is a direct process, while segregation is indirect; however, for metals having high carbon solubility (such as Ni and Fe), some carbon atoms will always diffuse into the hot substrate. As the substrate cools down, the dissolved carbon will segregate to the surface contributing to graphene growth.

Many transition metals (Ni, Co, Ru, Ir, Pt, Cu) have successfully been used to catalyze the formation of graphene. Their catalytic properties come from the partially filled d-orbitals and are enhanced by the formation of intermediate carbon containing compounds. The growth mechanism is substrate specific and depends on many characteristics such as carbon solubility, exposed crystallographic face, and surface cleanliness. This complicates the analysis of the processes involved and, in fact, very little is established up to now on the influence of all these factors, as for example the role of transition-metal carbide contamination in graphene formation. It has indeed been observed that on Ni(111) the growth of an ordered, single layer thick, Ni_2C phase competes with graphene growth (Jacobson 2012; Jorio 2012; Lahiri 2011). On the other hand it has been argued that graphene growth by CVD on group IVB-VIB metals is facilitated via carbide formation (Zou 2014).

Being dependent on many factors, the graphene growth can be optimized by tuning several variables: the hydrocarbon used in the reaction (CH_4, C_2H_4, C_6H_6, …), the gas flux/pressure, the ratio of hydrocarbon and additional gases (Ar, H_2, O_2), the substrate temperature, after growth annealing processes, cooling rate etc. A direct industrial interest is driving research to obtain high quality and large area graphene films on nickel, copper and other substrates.

Copper foils have been largely employed in CVD synthesis thanks to their low cost and to the relatively mild growth pressure and temperature required: temperatures ranging from 800 to 1050 ^{o}C and ethylene or methane are usually employed.

Ni(111) is the metal single crystal surface having the smallest lattice mismatch with graphene (about 1.3%), and the interaction with the matching substrate is particularly strong. The growth on metallic single crystals requires previous surface cleaning, by standard cycles of ion sputtering (argon or neon ions) and annealing at high temperature (details are given in the experimental section).

Graphene can then be prepared by thermal dehydrogenation of hydrocarbons on the surface. In a typical preparation recipe, the substrate is heated to 550 °C and exposed to a pressure of 10^{-7} to 10^{-6} mbar of ethene (C_2H_4) in Ultra High Vacuum (UHV) for approximately 10 minutes. The preparation temperature is lower than the one needed for copper due to the higher chemical reactivity of nickel, and it influences the properties of the resulting film. At lower temperature nickel carbide is formed, while higher temperature can be used only for carbon-enriched samples. In the latter condition a significant increase of rotated graphene on carbide domains are observed, which are ascribed to graphene grown on carbide (Jacobson 2012). Further increasing the preparation temperature leads to the production of multilayer graphene.

Due to the small lattice mismatch graphene forms a (1x1) structure on Ni(111). Different possible configurations are, however, possible depending on the relative position of the carbon atoms with respect to the underlying nickel (Zhao 2011).

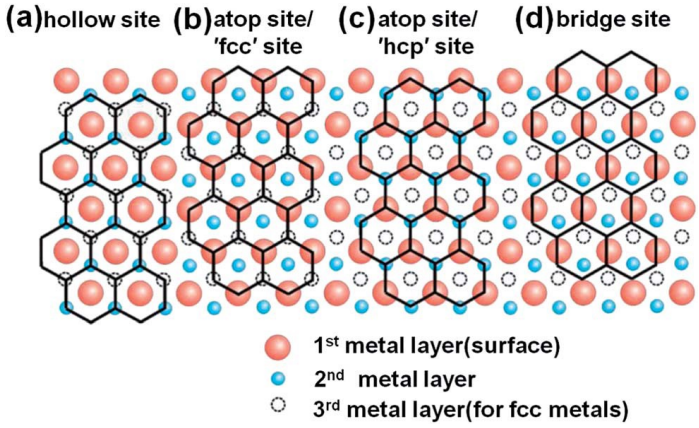

Figure 3 – The four different basic adsorption configurations of a honeycomb lattice on a matching hexagonal densely packed metal surface. Taken from(Dahal 2014).

I report in Fig. 3 the main structures:

a) *hollow or fcc-hcp*: both carbon atoms are in hollow position with respect the substrate (one on top of the atoms belonging to the second nickel layer and the other one of the atoms belonging to the third nickel layer).
b) *top-fcc*: One carbon atom is on top of the atoms belonging to the first nickel layer and the other has the same position of the nickel atoms belonging to the third layer.
c) *top-hcp*: one carbon atom is in on top position while the second atom occupy the same position of the atoms belonging to the second nickel layer.

d) *top-bridge bridge*: one carbon atom is placed in bridge position over first and the second nickel layers, while the second carbon atom is placed in bridge position between the atoms of the first and the third layer.

Besides these configurations, that strongly interacts with the substrate, in Near Ambient Pressure (NAP) it is possible to find the graphene in a configuration more weakly bonded with the substrate and in a detached state (Fu 2017).

The main structural features are the 2.11 Å interlayer distance between graphene and the topmost Ni atoms and the very small corrugation of the graphene layer (0.05 Å between the two carbon atoms of the graphene lattice). This small interlayer distance, compared to graphite interlayer distances, results from the strong interaction between C and Ni atoms at the interface. The electronegativity difference of C and Ni causes a strong *n*-doping of graphene due to electron transfer from the Ni 4s to the G π states. Angle resolved photoemission electron spectroscopy (ARPES) inspection clearly shows the hybridization of Ni d states and the G π band with the consequent destruction of the Dirac cone (Dedkov 2015).

CO reactivity and under cover chemistry

As discussed previously, one of the most promising and developed technology to produce graphene (G) at industrial level is to obtain the structure on reactive substrates, usually by hydrocarbon dehydrogenation at high sample temperature. In my work I show that G can be grown on Ni(111) by CO exposure at NAP conditions and at T=500 K, i.e. at a temperature significantly lower than the one needed when using hydrocarbons as C source.

CO exposure at 600 °C is known to lead to graphene formation on Ni (110) (Monachino 2014), a process which implies either CO dissociation at defects of the Ni surface or the onset of the Boudouard reaction

$$CO + CO \rightarrow CO_2 + C \qquad \textit{Equation 1}$$

in which two CO radicals react to CO_2 leaving one carbon atom at the surface. The latter process is employed in industry on bare Ni surfaces (Bost 2016) but there is still little evidence for its occurrence under controlled laboratory conditions since it is favoured by high pressure. In most catalytic reactions the production of elemental carbon is undesired since it leads to the poisoning of the catalyst (coking), but it can be usefully exploited e.g. for the production of carbon nanotubes

on Ni supported on MgO (Chen 1997) as well as on Co (Chen 2006). Formation of graphene has been reported also on Co nanoparticles exposed to CO at atmospheric pressure (Heintz 1989) via the Boudouard reaction, which is known to occur as well on other transition metals such as Ru (Panagiotopoulou 2011).

Lower reaction barriers are expected for CO on Ni than for other reactive metals, such as Co, Fe, Cr and Ti (Blomberg 2013) because of the lower adsorption energy. The Boudouard reaction is exothermic by ~ 1.77 eV/molecule (Han 2013; Hunt 2013) under standard conditions and occurs only up to temperatures for which the free energy is dominated by the entropic term. The reaction constants at equilibrium, K_{eq}, are given by (Snoeck 2002):

$$K_{eq} = e^{\frac{-160.8}{R}} e^{\frac{180965}{RT}} \qquad \textit{Equation 2}$$

for graphite formation (2) and by

$$K_{eq} = e^{\frac{-160.8}{R}} e^{\frac{133100}{RT}} \qquad \textit{Equation 3}$$

or carbide formation (3) where R is the gas constant expressed in the international system and T the temperature in K. The equilibrium constant is unitary around 937 K.

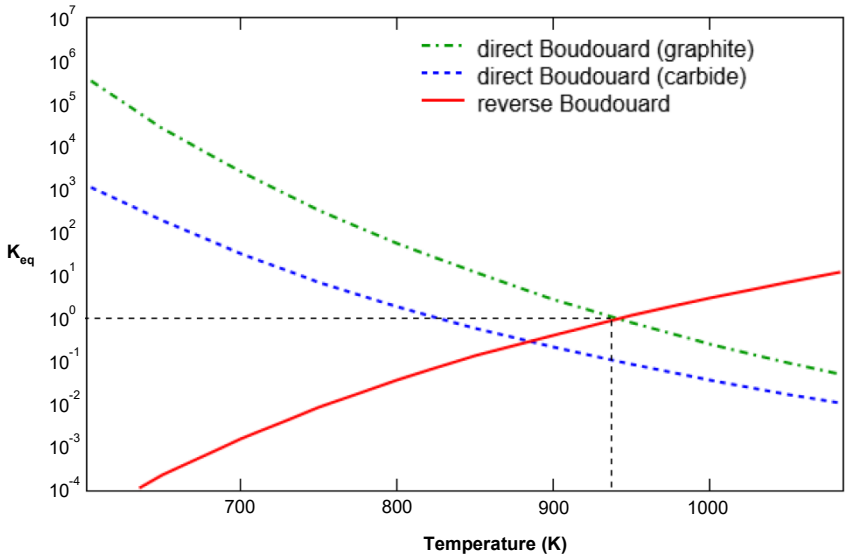

Figure 4 - Temperature dependence of the equilibrium constant for the unsupported graphite (green, dash-dotted line) and carbide (blue, dashed line) formation and the reverse (red, solid line)

Boudouard reaction. The reversing of the reaction direction at atmospheric pressure occurs at 937 K when graphite is involved. Data taken from ref. (Snoeck 2002).

Above such T the Boudouard equilibrium is reversed yielding CO from CO_2 and C. Such reaction conditions are used e.g. for the high temperature gasification of coal (Han 2013). It is also apparent that graphitic carbon formation is thermodynamically favoured with respect to nickel carbide.

A recent Near Ambient Pressure (NAP) X-Ray Photoemission (XPS) study performed on Ni(110) has shown that dosing CO at 0.03 mbar yields a nearly oxygen-free surface covered with several carbon-containing species, including graphene (Monachino 2014). Similar conclusions were drawn in another more recent investigation in which Ni(110) was exposed to CO at 0.01 mbar (Roiaz 2016). These results can be explained either by CO dissociation (followed by fast oxidation of the oxygen adatoms by a further CO molecule from the gas phase) or by the onset of the Boudouard reaction. However, which one of these two possible paths matters remains unclear.

Hammer et al. (Hammer 1997) calculated the enthalpy change occurring in the dissociation reaction to be about 0.41 eV/molecule with respect to gas phase CO. This reaction is thus less exothermic than the Boudouard reaction and can proceed only at defects of the Ni surface. Which reaction actually occurs depends thus critically not only on the pressure of the reactants and on temperature but also on kinetic factors, i.e. on the activation barriers for the two competing processes. Experimentally, the barrier for CO dissociation on Ni has been estimated to be around 1 eV/molecule (Nakano 2000), i.e. about 0.4 eV/molecule higher than the theoretical forecast. The barrier for the occurrence of the Boudouard reaction has been estimated by Density Functional Theory (DFT) to be about 3.4 eV/molecule (Blaylock 2009). However, if the real barriers were so high, the reaction rate would be strongly suppressed, contrary to experimental evidence.

Indeed, the disproportionation reaction occurs with probabilities of 10^{-4} and 10^{-2} on Ni(100) and Ni(110) (Ni 1989; Rosei 1983), respectively. Subsequent experimental studies of the Boudouard reaction on Ni found the much lower activation barrier value of (0.133 ± 0.066) eV/molecule for Ni(111) and even a negative value for Ni(977) (Nakano 2000). For the latter surface it was suggested that the disproportionation reaction involves firstly the dissociation of adsorbed CO and then the reaction of the so-produced oxygen with another CO molecule, the fingerprint of the occurrence of dissociation being the presence of atomic oxygen at the surface at 350 K, i.e. when the C uptake is largest.

In the present study I investigated CO adsorption on Ni(111) upon CO exposure at a pressure P_{CO} ~ 2 mbar, i.e. in a range significantly higher than the one used in previous studies on Ni(110) (Monachino 2014; Roiaz 2016).

The choice of Ni(111) rather than Ni(110) is motivated by the fact that this is the most commonly used substrate for graphene growth. The substrate-graphene distance (2.13 Å) is only slightly larger than for Ni (110) but intercalation underneath the graphene sheet is easier since the calculated adsorption energy of monolayer (ML) graphene on the substrate (164 meV/atom) is lower than for Ni(100) and Ni(110) (180 meV/atom and 209 meV/atom, respectively). Graphene on Ni(111) is therefore the ideal candidate to study chemistry under cover.

The higher CO pressure is expected to favour the Boudouard reaction mechanism over CO dissociation due to the quadratic dependence of the equilibrium constant on the CO partial pressure in the gas phase. Indeed, I observed graphene formation at temperatures at which segregation of dissolved carbon is still inhibited (it sets in at 400–600 ◦C (Africh 2016)), excluding this process to be important in the present experimental conditions. Indeed, graphene growth by C segregation in Ultra High Vacuum conditions (UHV) occurs only above 650 K.

As soon as large enough graphene patches have developed on the Ni(111) surface, a signal related to physisorbed CO_2 is detected. Given the high substrate temperature, the latter can only correspond to intercalated molecules and is indicative that CO_2 formation has occurred under the graphene cover. It is noticeable that in this experiment I obtained the graphene structure mostly in the weakly interacting and detached state. This observation is crucial, in fact one of the main drawbacks of the graphene production on a supporting metal catalyst is that the presence of the substrate affects the transport properties of the G layer. In particular, when G is strongly interacting with it, as in the case of G/Ni (Africh 2016; Del Puppo 2021) and G/Ru (Gyamfi 2011), the Dirac cone is altered so much to destroy the Dirac cone and thus the exceptional mobility of the charge carriers. A promising way to decouple G from the underlying substrate and to restore its peculiar electronic properties is intercalation of atoms (Dong 2017) and molecules (Fei 2015), a phenomenon that is therefore thoroughly investigated.

Confinement of molecules under the G layer is also interesting for the purpose of sensoristics and catalysis. On the one hand, the change in the electronic properties of graphene can be used a probe of adsorption; on the other hand, chemical reactions may be affected by the spatial confinement of the reactants if they take place below the graphene cover. E.g., the G overlayer is known to weaken the interaction between CO and Pt(111), thus reducing the activation barrier for its oxidation (Yao 2014). Therefore, the interfaces between G and metal surfaces may act as 2D confined nanoreactors, in which catalytic processes are promoted (Dong 2017). The feasibility of

this approach was also demonstrated for CO oxidation on G-covered Pt nanoparticles (Gao 2016) and for methanation on h-BN-covered Ni nanoparticles (Gao 2016).

An experimental study of CO intercalation under G/Ni(111) has been recently performed by Wei et al. by Near Ambient Pressure X-ray Photoemission Spectroscopy (NAP-XPS) (Knop-Gericke 2009; Wei 2015) in operando conditions up to 0.1 Torr. Exposure to 5 Torr has been reported as well, but with XPS inspection performed only after the evacuation of the experimental chamber. The authors find that CO intercalation occurs under a complete G layer, with CO ending up mainly at bridge sites with only a minor component at atop sites. Therefore they conclude that, under the G cover, CO behaves in a similar way as on a bare Ni(111) surface under Ultra High Vacuum (UHV) condition and at room temperature (RT) (Held 1998). Upon annealing, partial de-intercalation of CO occurs at around 350 K, but a significant amount of intercalated CO persists even after annealing to 473 K. As expected, the initially strongly interacting G layer detaches from the substrate due to intercalation, giving rise to lower energy XPS components (weakly interacting and detached graphene). In my work I eviscerate what occurs to the system at 4 mbar in operando conditions: CO exposure on a G/Ni(111) layer, grown by ethene dehydrogenation, leads to CO_2 accumulation under the G cover and allows for the onset of the Boudouard reaction already at 340 K. New physics is therefore disclosed by exploring this so far untrodden pressure range.

3. Experimental

Near Ambient Pressure Photoelectron Spectroscopy

X-ray Photoelectron Spectroscopy is an analysis technique based on the photoemission of core electrons induced by X-rays. Upon X-Ray exposure several processes occur: photoemission, Auger electron emission, electron-hole pair creation and inelastic scattering events.

As illustrated in Fig. 5, in the photoemission process a core electron absorbs the energy of the X-Ray and is promoted from to a free state in the conduction band above the vacuum level. The electron is eventually photoemitted with a kinetic energy, E_K, related to its Binding Energy, E_B, by the Einstein equation:

$$E_K = h\nu - E_B - \phi \qquad \textit{Equation 4}$$

where ϕ is the work function of the material and $h\nu$ is the energy of the absorbed photon. Since $h\nu$ (and to some extent also ϕ) are known parameters, from the value of E_K direct information on E_B can be retrieved.

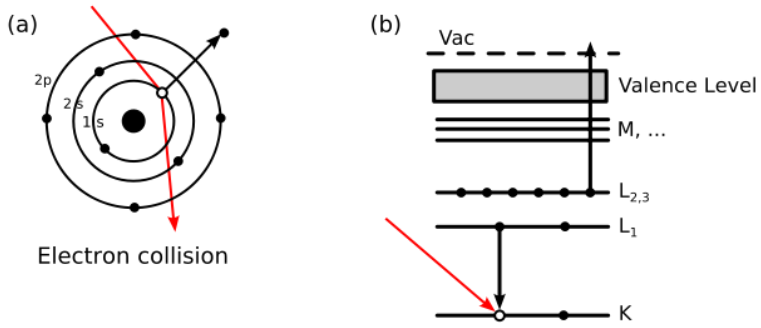

Figure 5 – Photoemission process: a) the photon (red arrow) is absorbed by a core level electron from the K shell and is emitted from its atom. b) the resulting hole may be filled by an electron falling from a higher energy shell. In the Auger process the released energy is transferred to another electron of the same shell which is then emitted with a kinetic energy characteristic of the involved atomic species.

The E_B values are characteristic for each atomic level and their analysis provides information about the chemical composition of the sample. Furthermore, the energy levels are influenced on a finer level by the chemical environment of the emitting atom. E_B measurements allow therefore to distinguish between atoms of the same kind in but different chemical environments. The electrons in the valence band are weakly bonded to the nucleus and thus are strongly influenced by their chemical environment. The core electron states follow their shift resulting in chemical shifts of the

order of up to several eV. Such core level shifts allow, e.g., to distinguish between the carbon in graphene layer (E_B del C 1s 285.0 eV (Wei 2015)) from the carbon forming of nickel carbide (E_B=283.4 eV (Wei 2015)).

Despite X-Rays penetrate in the materials for microns the photoemitted electron (having energies of 100 eV to 1000 eV) interact very strongly with the substrate atoms and the depth from which they can be emitted is limited to few atomic layers (see universal curve for the mean free path in a solid reported in Fig. 6). XPS is thus a surface sensitive technique: only the electrons photoemitted in proximity of the surface can leave the sample and be detected. The surface sensitivity can, moreover, be further enhanced by collecting the photoelectrons at grazing emission angles.

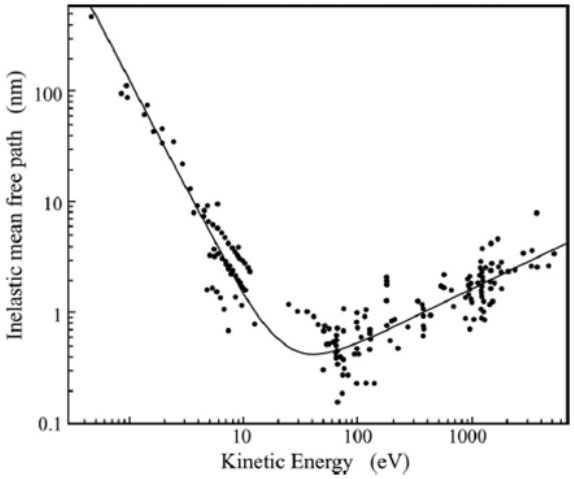

Figure 6 – Electron inelastic mean free path as a function of the electron energy.

XPS is a quantitative technique: the intensity of the photoemission peaks is proportional to the number of atoms of a certain species excited by the beam and, taking into account the sensitivity factors for each element, it is possible to estimate the concentration of such species. Photoelectron diffraction and calibration problems may, however, limit the attainable accuracy.

Experimental apparatus

The experiments have been performed at the TEMPO beamline of the SOLEIL synchrotron radiation source (Saint-Aubin, France) which is equipped with the NAP-XPS facility of Sorbonne Université. The set up allows measurements from UHV conditions up to 20 mbar CO. A differentially pumped entrance is used to let the X-ray beam into the chamber. The photon beam diameter is 0.1 mm. The beam impinges on the sample at an angle of 54° with respect to the sample normal. The NAP-XPS analyser (Specs Phoibos 150 NAP) consists of four separate pressure stages separated by apertures. The first pumping stage, hosting the wide-angle pre-lens of the analyzer, is separated from the

chamber by a conically shaped nozzle pierced with a 0.3 mm diameter hole that maximizes the efficiency of differential pumping. In the analyzer stage, the pressure is reduced by five orders of magnitude with respect to the one in the main chamber. To limit the attenuation of the photoelectron signal by scattering off the s phase, the nozzle is placed very close (at a distance of <1 mm) to the sample surface (Liu 2019).

During the experiments, the pressure in the chamber was kept constant using a leak valve to compensate for the pumping action of nozzle and beam entrance, all other connections to pumping systems being closed by valves.

The sample is mounted on a sample holder and can be heated with a ceramic heater botton. The Ni(111) surface was cleaned by sputtering cycles with 3 keV Ar^+ ions followed by annealing to T~ 1000 K in UHV and by exposing the sample to $5 \cdot 10^{-7}$mbar of O_2 at 1000 K for 10 min. This procedure led to a surface clean of contaminants but for some Ni carbide that could not completely be removed in the limited time available at the beamline.

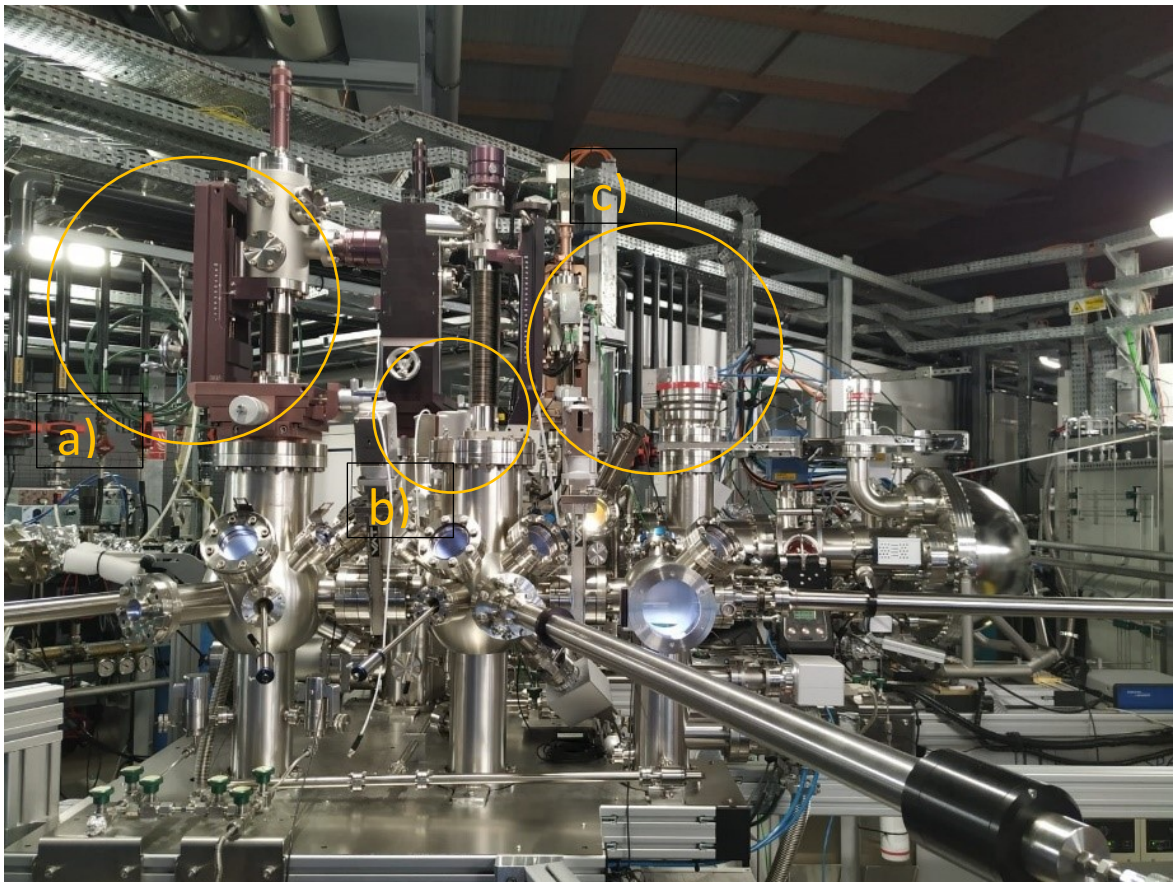

Figure 7 - Experimental apparatus at the TEMPO beamline of the SOLEIL synchrotron radiation source (Saint-Aubin, France) with the NAP-XPS facility of Sorbonne Université: a) sputtering chamber; b) main chamber hosting the NAP-XPS; c) NAP-XPS analyser (Specs Phoibos 150 NAP).

A set of electrostatic lenses collects, focusses and accelerates the photoemitted electrons towards the hemispherical analyzer.

Since the photoemitted electron flux is attenuated by collisions with the gas molecules, usually XPS is carried out in UHV. In this regime good signal intensities are obtained, but the required very low pressure becomes a big limitation for the in-operando investigation of catalytic processes. It is in fact recognized that for the study of many important interface phenomena, investigations under at least near ambient pressure conditions are essential to overcome the so-called 'pressure gap', which arises from the difference of the chemical potential of a gas at typical ultrahigh vacuum conditions (10^{-9} mbar) as compared to realistic pressures in a technical process or in the environment (Trotochaud 2017). Catalysts for example are not static but dynamic (Papaefthimiou 2012), and the interaction with the gases involved in the reaction (both reactants and products) can dramatically affect their chemical composition and consequently their catalytic properties. Only since a decade the range of pressure of XPS investigations could be extended to the mbar region.

The XPS technique was implemented in the late '70 by K. Siegbahn's group in Uppsala (Siegbahn 1973; Siegbahn 1985) and were followed by other designs (Schnadt et al. 2012) all based on laboratory x-ray sources. In 1990s the first Synchrotron apparatuses were developed (Ogletree 2002; Bluhm 2004). Eventually, commercial systems became available and the technique could spread becoming widely available (Shavorskiy 2014; Weatherup 2011; Knop-Gericke 2009; Crumlin 2013).

Most of the current NAP-XPS instruments consist of a sample chamber that can be backfilled with a gas or gas mixture. Electrons (and gas molecules) enter the differentially-pumped electrostatic lens system of the spectrometer through a small aperture (<1mm diameter). The sample is brought close to the aperture to reduce the path length of the electrons through the high pressure regions. Several differentially-pumped electrostatic lens stages convey the electrons to the entrance of a hemispherical electron analyzer and maintain high-vacuum conditions around the electron detector at the exit of the hemispherical analyzer.

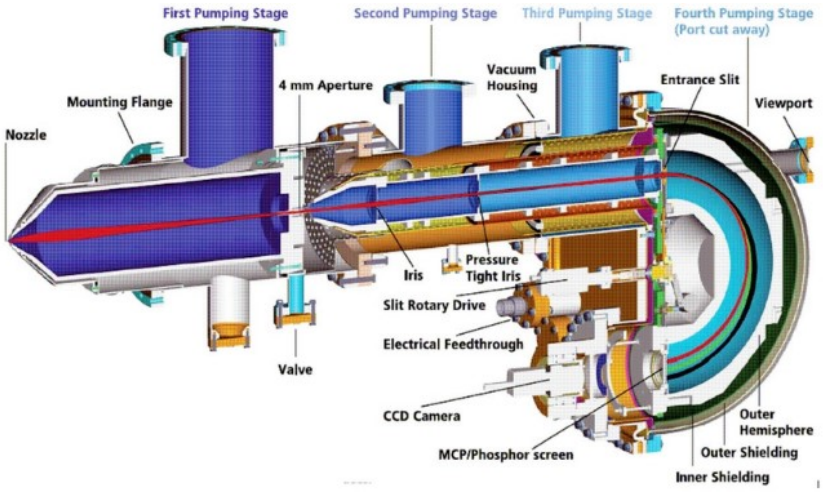

Figure 8 - Scheme of the NAP-XPS analyzer.

Typical sample cell pressures in NAP-XPS are in the mbar range. The x-ray source itself must also be operated at UHV, and thus incident photons pass through an x-ray transparent window (typically SiNx or a thin aluminum foil) or a differential pumping stage that physically separates the gas environment from the UHV photon source (either lab-based anode or synchrotron beamline).

Data analysis and sample preparation

In the present experiment Graphene was grown by exposing the sample at T=830 K to C_2H_4 at = 1.7 10^{-5} mbar for 300 s, corresponding to ~ 3800 L following the procedure described in ref. (Celasco 2017).

Selected spectra of the C 1s region recorded during growth are shown in Fig. 9. We notice that the intensity of the C 1s peak due to graphene is lower at the end of the exposure (green trace) than after cooling the sample (blue trace). This indicates that, while most of the G layer forms by ethene dehydrogenation, full monolayer coverage is attained only by C segregation during the cooling process. A more detailed inspection of the data shows that such process occurs between T=830 K and 580 K, below which temperature no further change occurs in the C 1s intensity.

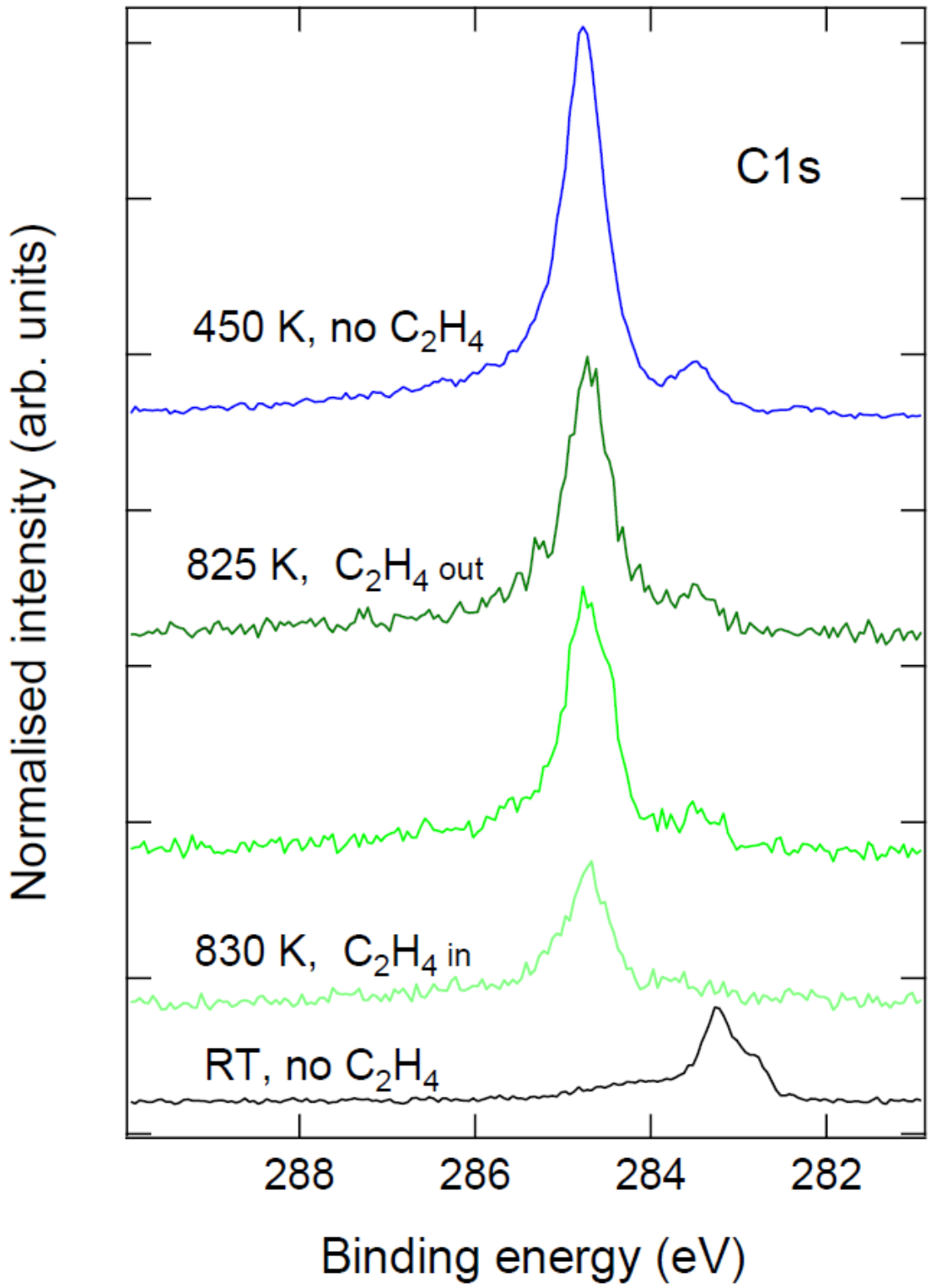

Figure 9 - C 1s spectra recorded during graphene growth by ethene dehydrogenation. Photons of 400 eV have been used to achieve a high sensitivity to carbon. Intensities were normalized on the background.

At room temperature surface that contains carbide islands which could not be removed by sputtering during the beamtime, as witnessed by the feature at 283.4 eV (black spectrum). Upon increasing the temperature up to 830 K and dosing ethylene (from light green to dark green) I

observe the appearance and the growth of the graphene structure with a centroid around 284.7 eV. In the blue spectrum, recorded after the cooling down of the system, I observe a further increase of the graphene structure due to segregation.

Unless otherwise specified, XPS inspection of the carbon and oxygen regions has been performed at a photon energy of 650 eV to examine both regions with the same monochromator gap. The photon energy of 970 eV was used for the Ni 2p region (not shown, recorded for control purpose). The XP spectra were acquired sequentially using photon energies of 650 eV to inspect C 1s and O 1s regions and of 970 eV for the Ni 2p regions, respectively.

Since the transmission function of the analyzer is constant, under UHV conditions the relative O 1s and C 1s sensitivities are determined by the corresponding photoemission cross-sections $б_{C1s}$ = 1.5 Mb; $б_{O1s}$ = 3.5 Mb) (Yeh 1985). However, for the spectra acquired at NAP conditions, also the electron kinetic energy dependent attenuation of the signal due to the gas phase species had to be considered. The latter depends on the gas density between sample and analyzer and thus on background pressure and crystal temperature. Since the mean free path is larger at higher kinetic energy of the electrons, the O 1s line is more heavily affected than the C 1s line. In order to fit self-consistently the O 1s and C 1s regions, I firstly determined the intensities of the different O 1s components and then I fitted the C 1s region, imposing that the intensity of each of the adsorbed species I_{C1} satisfies the relationship:

$$I_{O1s\ ads} / I_{O1s\ COgas} = \varepsilon\ I_{C1s\ ads} / I_{C1s\ COgas}. \qquad \textit{Equation 5}$$

where ε is 1 for CO and 2 for CO_2; $I_{O1s\ ads}$ is the intensity of the O 1s line of the corresponding adsorbed moiety while $I_{O1s\ gas}$ and $I_{C1s\ gas}$ are the intensities of the corresponding lines for gas phase CO. The possible change in the O 1s/C 1s intensity ratio between gas phase and adsorbed species due to photoelectron diffraction is not taken into account (Vesselli 2008).

The recorded spectra were analyzed with the KOL-XPD software. Doniach Sunjic functions convoluted with a gaussian and a Shirley background were used to fit the main C 1s line, ascribed to graphene, to determine its asymmetry. Where not explicitly discussed, an asymmetry parameter of 0.1 has been adopted, a value set also in most of the papers in literature (Blume 2015; Susi 2015). The C 1s width parameters (Lorentzian width = 0.23 and Gaussian width = 0.36) have been experimentally determined by fitting the clean graphene carbon spectrum (Fig. 10), in which the

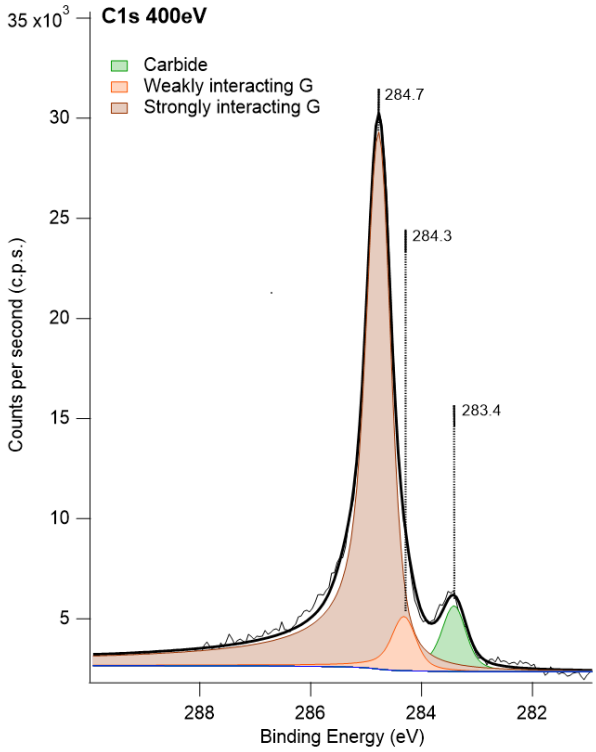

Figure 10 – C 1s spectra recorded during graphene growth by ethene dehydrogenation. Photons of 400 eV have been used to achieve a high sensitivity to carbon. Intensities were normalized on the background.

number of components was smallest compared to the rest of the spectra. From the fitting emerge in fact only three components: top-bridge graphene (284.7 eV) weakly interacting or rotated graphene (284.3 eV) and nickel carbide (283.4 eV).

The shape parameters of the different components, have been kept constant for the spectra recorded for all preparations. During each experiment I also fixed the BE of the species using a two-step procedure: 1) first the BEs have been left free to vary over a range of 200 meV; 2) the analysis has been eventually refined imposing the average value of the BEs determined from the previous analysis of all spectra for each component.

Voigt functions were sufficient to describe all peaks other than graphene. To determine the most appropriate line shape of the oxygen species, I made reference to the UHV spectra acquired on bare Ni(111) partially covered by carbide islands (Cfr. Chapter 4, Fig. 11, I). In these conditions the bare NI(111) surface is rapidly saturated by the residual CO present in the rest vacuum of the UHV chamber, producing an intense and well characterized signal at 532.2 eV due to adsorbed CO_{top} and at 531.0 eV due CO_{bridge} (Wei 2015). The fitting, which includes also a minor contribution due to atomic oxygen at 529.6 eV, has been performed allowing for a variation of the parameters describing the width of the Gaussian as well as of the Lorentzian components, obtaining values of

1.4 and 1.2, respectively. These widths have been taken as a reference for the adsorbed O 1s species and kept constant in the analysis of all the other spectra in the other experiments.

A linear background was used for the O 1s region. All binding energies (E_b) are calibrated with respect to the Fermi edge of the Ni sample, which was acquired for control for each set of experiments.

In order to support the correctness of the fitting procedure and the existence of the identified compounds, the assignation of the possible species that could be reasonably be present in the system under study has been taken into consideration and, if necessary, excluded after a careful analysis of the spectra.

For graphene grown on Ni(111) a BE of 283.7 eV (Celasco 2017) has been reported in literature. To describe it, I introduced a component with BE between 283.6 eV and 283.8 eV. During the fitting procedure of each spectrum series, I observed a systematic suppression of the corresponding signal under NAP conditions and thus I excluded the presence of dissolved carbon in appreciable amount. Other possible species that could have formed upon the experiment are carbonates. However, the presence of these compounds has been inconvertibly excluded since I never observed any signal at their characteristic BE of 298.4 eV in C 1s region.

I also considered the possibility of water contamination. This molecule, if present, could dissociate and generate a signal at 532.2 eV due to adsorbed OH in O 1s region. Despite some intensity has been detected in that region the presence of OH is justified only in trace amounts. In fact a not negligible signal has been observed only under CO NAP pressure conditions, but its assignment to OH contamination is then ruled out because in the presence of water in the gas-phase a peak should be evident at E_B(O 1s)=536.0 eV (Patel 2019), contrary to experimental evidence which shows in the relevant spectral region an intensity lower than 1% of the one of gas-phase CO. Water intercalation followed by dissociation is not possible at such low partial pressures (Cfr. Chapter 5, Fig. 16).

Finally, by an inspection of the Ni $2p_{3/2}$ spectra it has been possible to rule out the presence of tetracarbonyl-nickel in appreciable amounts since the corresponding features at 854.4 eV and 854.8 eV (Africh 2016) are missing in the Ni $2p_{3/2}$ spectra at least within our experimental sensitivity (Cfr. Chapter 5, Fig. 22).

Thanks to the high resolution of the synchrotron radiation has been possible to discern between the major graphene components and reproduce the graphene peak in terms of relative percentages (Celasco 2017). To the best of my knowledge, besides the species we addressed in this work (Cfr. Chapter 4, Table 1), whose interpretation will be deepened in the following, no further compounds mentioned in literature could reasonably be present in the experimental spectra.

The same constatations held for all the experiments I performed and thus assume a general validity in the present work.

Finally, the intensities of the C 1s components of the oxygen containing adsorbed species (CO and CO_2) is constrained by the intensity of the corresponding O 1s peak according to eq. 5, thus granting the reliability of the fitting in the tail of the graphene component which overlaps with lower intensity CO related peaks.

The coverage (expressed in ML of the Ni(111) substrate) of the different species has been determined by comparing the corresponding C 1s intensity (normalized to the background) to the one recorded at the same photon energy for single-layer graphene grown by ethylene exposure (2 MLs of the Ni(111) substrate).

Under NAP conditions, the presence of photoemission intensity due to the gas phase species enables to track also work function changes $\Delta\Phi$ of the sample by the apparent binding energy E_b of the gas phase specie. Indeed, the latter is linked to the vacuum level rather than to Fermi Level. The apparent shift of such lines Δ(BEFL) is thus given by:

$$\Delta\Phi = -K\cdot \Delta BE_{FL} \text{ (gas-phase)} \qquad \textit{Equation 6}$$

with K being a constant close to unity. This relation holds because the relevant gas molecules are at the same potential as the surface due to the close proximity of the nozzle to the sample.

4. CO NAP exposure on Ni(111) partially covered with carbide islands

In the present chapter I investigated the interaction of CO with a Ni(111) sample partially covered with carbide by Near Ambient Pressure (PCO ~ 2 mbar) X-Ray Photoemission Spectroscopy. This study aims to mimic realistic graphene growth condition in presence of CO. Carbide is in fact often present on the nickel surface due to the difficulty of completely remove it.

Fig. 11 reports a series of XPS spectra recorded during CO exposure at P_{CO} ~ 2 mbar on the Ni(111) surface in the temperature range 305 K ≤T ≤ 550 K.

Initially, the sample is at T = 305 K and in UHV (lowermost spectrum). Different peaks are evident both in the C 1s and O 1s regions. The photoemission lines are assigned according to previous literature and listed in Table 1.

The feature at 283.4 eV is due to 0.1 monolayer (ML) of carbon in nickel carbide, which covers thus approximately 20% of the surface. Adsorption from the residual vacuum has occurred on the bare part of the Ni(111) surface, as witnessed by the peaks at 285.4 eV and 531.0 eV and at 286.0 eV and 532.2 eV, corresponding to CO chemisorbed at bridge and on top sites, respectively. Additional contributions due to CO adsorption on the Ni_2C patches (at 286.4 eV and 532.6 eV for CO_{top} and at 286.0 and 531.4 eV for CO_{bridge}, respectively) are also expected. Their coverage under UHV is, however, negligible due to their lower heat of adsorption(Wei et al. 2015). Adsorbed CO consists mostly of bridge bonded molecules. The very minor contribution at 529.6 eV is due to an atomic oxygen contamination.

CO is eventually introduced into the chamber at a pressure of 2.15 mbar (see spectrum II) while keeping the sample at room temperature, RT. The small feature due to atomic oxygen disappears immediately, probably due to its removal by CO oxidation.

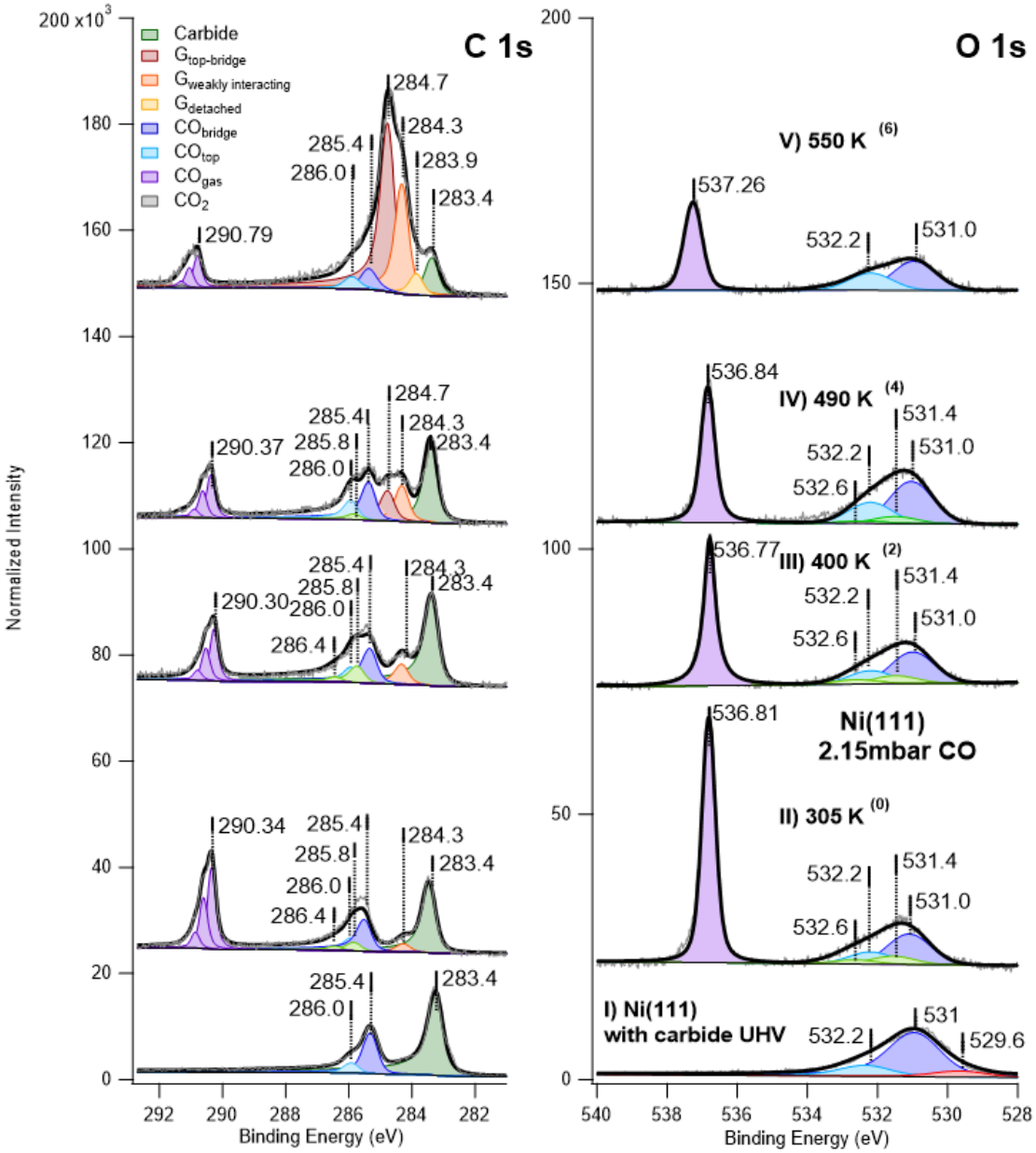

Figure 11 - XPS C 1s and O 1s regions recorded at a photon energy of 650 eV on Ni(111). Bottom spectrum: initial conditions with partial carbide coverage recorded in UHV (I). The bare part of the surface is populated by adsorbed CO. The other spectra correspond to different exposure times at 2.15 mbar CO. Adsorption on nickel carbide (peak at 283.4 eV) is initially visible and disappears when heating the sample above 490 K. The additional peaks around 285.0 eV witness the formation of graphene. The spectra correspond to the different temperatures: II) 305 K; III) 400 K; IV) 490 K; V) 550 K. The numbers in brackets refer to the numbering in the sequence of spectra reported in Fig. 14.

*Table 1 - Binding energies of the species addressed in the paper; The * indicates assignments used in the present thesis.*

Species	**C 1 s (eV)**	**O 1 s (eV)**
Nickel carbide (Ni_2C)	283.4 (Wei 2015) ;*	
Detached graphene	283.9 (Wei 2015) ;*	

Weakly interacting graphene	284.3 (Wei 2015) ;*	
Top-bridge graphene	284.8 (Wei 2015) ;*	
CO bridge /Ni(111)	285.4 (Wei 2015) ;*	531,0(Wei et al. 2015);*
CO top /Ni(111)	286.0 (Wei 2015) ;*	532.2(Wei et al. 2015);*
CO bridge /Ni2C	285.8 (Wei 2015) ;*	531.5(Wei et al. 2015);*
CO top /Ni2C	286.4 (Wei 2015) ;*	532.6(Wei et al. 2015);*
CO_2 physisorbed	291.3 *	533.4*
	291.3 (Kamath 1984)	535.1 (Kamath 1984)
	290.6 (Vesselli 2008)	534.0 (Vesselli 2008)
CO_2 chemisorbed/ Ni(110)	286.2 (Ding 2007)	530.6 (Ding 2007)
Atomic oxygen		529.6–529.8 (Monachino 2014)
Surface oxide		530.2–530.4 (Monachino 2014)

From the second spectrum on the experiment is performed under NAP conditions. Additional peaks due to gas phase CO are therefore visible at 290.3 eV and 536.8 eV. The CO_{gas} peak in the C 1s region has a triangular shape due to the inelastic losses associated to the excitation of the CO stretch motion. The intensity of such peaks depends strongly on the sample temperature since the latter affects the gas density in proximity to the crystal surface.

Upon NAP CO exposure at RT intensity builds up at 284.3 eV, witnessing the formation of weakly interacting graphene on Ni(111). Contrary to what was observed in UHV conditions, additional peaks at 285.8 eV in C 1s and 531.4 eV in O 1s regions (Wei 2015) indicate that CO adsorption takes now place at carbide bridge sites (Wei 2015). We note that no further signal is present in the O 1s region except for those associated with adsorbed CO. In particular, the absence of atomic oxygen (expected at 529.6–529.8 eV (Monachino 2014)) or surface oxide (expected at 530.2–530.4 eV (Monachino 2014)) indicates that no CO dissociation has occurred.

Raising the sample temperature while maintaining the same CO partial pressure, P_{CO}, (spectra III and IV) causes an increase of the graphene-related signal in the C 1s region: at 490 K (spectrum IV), a peak form at 284.7 eV, a BE compatible with top-bridge graphene.

When the temperature is raised, the intensity of the top-bridge component of graphene grows further and, at T = 550 K, it becomes dominant over the weakly interacting one. Part of the carbon needed to build up the graphene layer must have come from the carbide phase, since the latter is

now reduced to a minor feature. This process also causes a decrease of ~ 0.4 eV of the work function, as witnessed by the corresponding upshift of the C 1s and O 1s components of CO_{gas}. The results shown so far are consistent with those previously reported for CO/Ni(110) (Monachino 2014) upon exposure to 0.03 mbar CO.

XP spectra recorded upon increasing the temperature to 600 K and above are shown in Fig. 12. The overall appearance in the O 1s region has now changed significantly. A feature has formed at 533.4 eV, which was absent on Ni(110) (Monachino 2014). It increases when raising T (spectra II and III) to 700 K and readily disappears upon evacuating the chamber at RT (not shown). This E_B value is compatible with physisorbed water as well as to O atoms covalently bound to carbon or CO_2. However, the former assignment is ruled out since a water coverage would rapidly decrease with increasing T (Li 2017), contrary to my experimental evidence. Furthermore, without formation of CO_2 it would be impossible to explain the growth of graphene already at 550 K. It is, indeed, well established in literature that C segregation off Ni(111) takes place above ~ 670 K (see e.g. ref. (Patera 2013)). The formation of the graphene layer below 600 K is, therefore, indicative of CO reaction to CO_2, leaving C atoms at the surface. Nonetheless, I have checked the behaviour of the Ni(111) sample (in presence of some carbide peak at 283.6 eV to mimic the starting condition of the sample) upon annealing in UHV conditions, to exclude the formation of graphene below 600 K. The result (see Fig. 12) shows that graphene formation by segregation is still negligible at 647 K and becomes evident only at 716 K, thus confirming that carbon segregation is negligible in our experimental conditions. Finally, the formation of species with O covalently bound to graphene is excluded since they should be stable upon evacuation of the experimental chamber, leaving CO_2 as the only option.

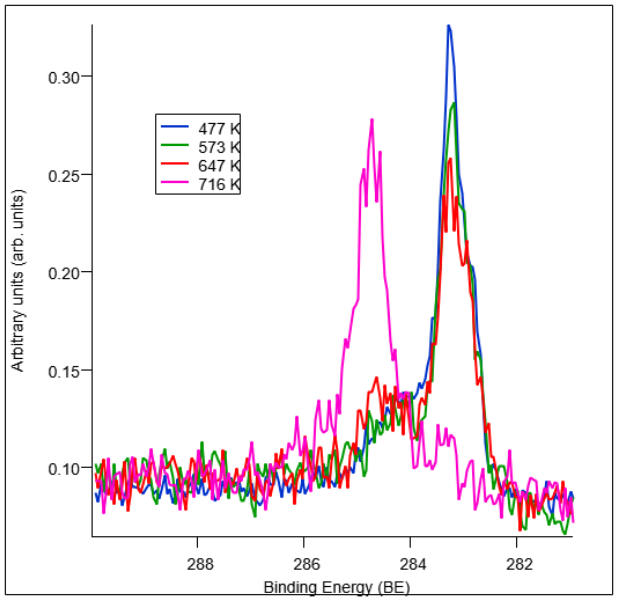

Figure 12 - Spectra recorded after annealing the Ni(111) sample partially covered with carbide (peak at 283.4 eV) in UHV to different temperatures: 477 K (blue); 573 K (green); 647 K (red); 716 K (pink).

The presence of physisorbed CO_2 is supported by the inspection of the C 1s region. I notice that the shape of the C 1 s peak of CO_{gas} has changed, developing a shoulder on the low BE side (see insets in the C 1s regions in Fig. 13). This shoulder cannot be due to a vibrational energy gain peak since it cannot account for more than 1,2% of its intensity even at T = 700 K. It is therefore indicative of another chemical species.

To evaluate its C 1s binding energy it, I set the C 1s gas peak position from the one of the O 1s gas phase peak (which has negligible vibrational contributions) and imposed the ratio of the intensities of such peaks to be the one of spectra recorded at a lower temperature when only CO_{gas} is present. The additional contribution needed for the fit comes out at 291.3 eV, a value close to the one reported for physisorbed CO_2 on Ni(110) (290.6 eV) (Ding 2007) and polycrystalline Ni (291.3 eV) (Kamath 1984). Given the experimental conditions (T=600 K) and the low adsorption energy of physisorbed CO_2, however, this species cannot accumulate at the surface. I conclude therefore that it is intercalated below the graphene layer which impedes its desorption. The constrained adsorption site as well as the different surface termination may account for the slightly lower E_B(O 1s) with respect to the value found by some of us for physisorbed CO_2 at bare Ni(110) (534.0 eV) (Vesselli 2008;Ding 2007). The E_B values for the physisorbed CO_2 in literature range indeed from 533.4 eV to 535.5 eV for the O 1s line and between 291.0 and 292.0 eV for the C 1s line on Cu surfaces (Kahk 2018) and read 534.9 eV and 291.3 eV for O 1s and C 1s lines, respectively, on Fe_3O_4 (Pavelec 2017).

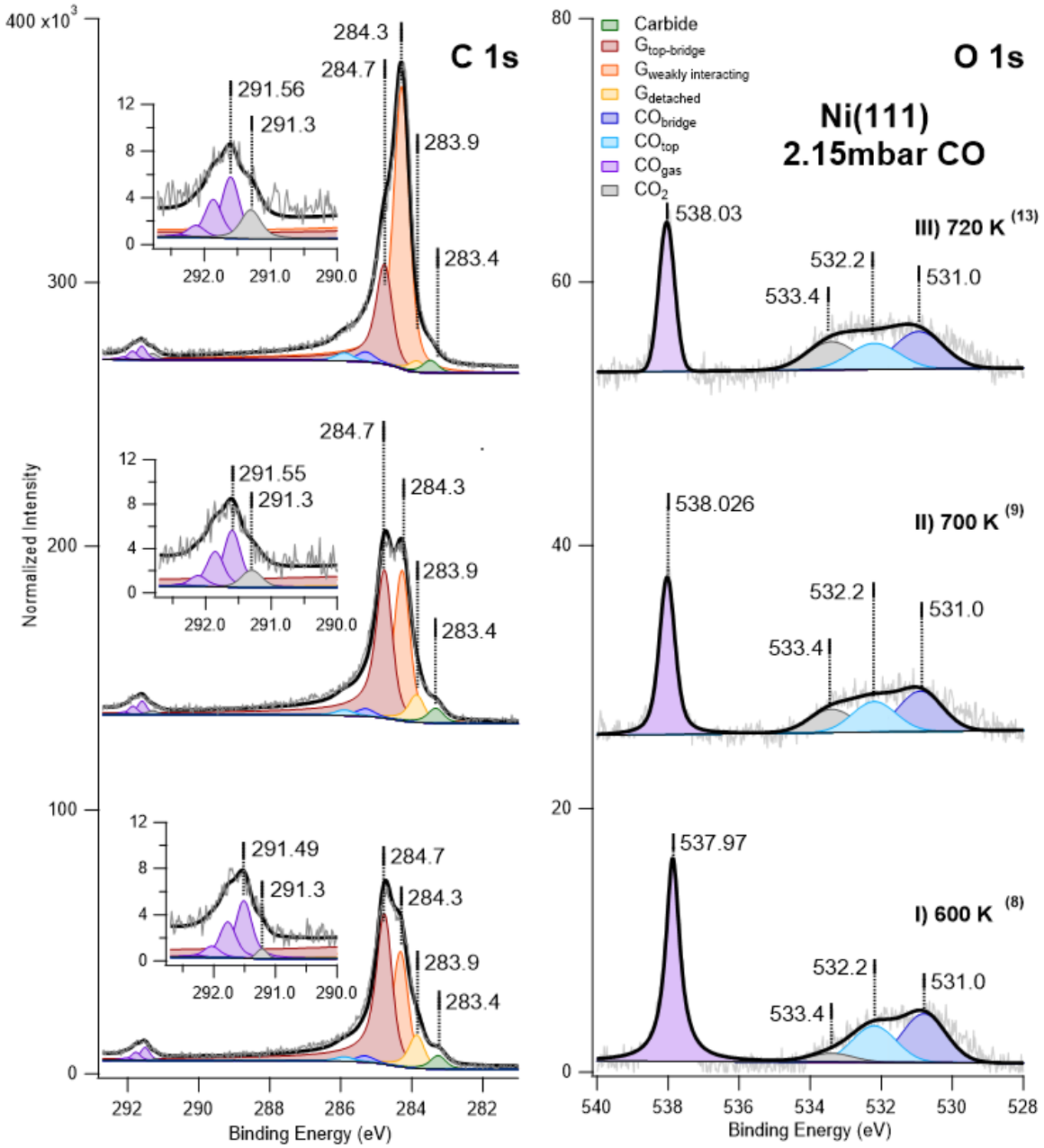

Figure 13 - C 1s and O 1s regions recorded at a photon energy of 650 eV upon further annealing the sample in 2.15 mbar CO pressure. The spectra were recorded sequentially at: I) T = 600 K; II) T = 700 K; III) T = 720 K. The C 1s panels contain insets with the enlargement of the region between 290.5 eV and 292.5 eV to highlight the presence of the additional peak at 291.3 eV. The numbers in brackets indicate the correspondence of the reported spectra with the sequence of Fig. 14. Note the difference in the C 1s and O 1s intensity scales.

Moving our attention to the other components of the spectra in Fig. 13, we note that, at 600 K, the CO_{top} component in the O 1 s region becomes almost as intense as the one in the bridge configuration. It is known that on Ni(111) at RT, saturation coverage of CO corresponds mainly to CO at bridge sites, which have been reported to dominate over top sites also for intercalated species below the graphene cover (Wei 2015). However, a Sum Frequency Generation study of CO adsorption on Ni(111) demonstrated that a high density phase can form at 130 K. CO occupies then

also on-top positions (Bandara 1998). The global CO intensity indicates a low coverage, but CO could have clustered reaching locally a high coverage. This may reasonably occur below the graphene sheet.

When the temperature is further raised to 720 K (Fig. 13 III), the ratio between the graphene-related peaks in the C 1 s region changes: the component due to weakly interacting graphene increases at the expense of top-bridge one. The CO and CO_2 signals show the same trend, suggesting that further intercalation has occurred, stripping off additional graphene patches from the substrate.

In order to better analyse the behavior of the system, in Fig. 14 I summarize the sequence of all spectra recorded in the experimental runs of Fig. 11 and 13. The top-panel reports the coverage of carbide and of the different graphene domains as well as the coverage of CO chemisorbed at bridge and top sites. In the determination of the coverage of intercalated species, I neglect the attenuation of the signal due to the graphene cover (when present, i.e. above 550 K), hence, the reported values for such species are actually a lower limit to the real coverage. The bottom panel shows the crystal temperature and the variation of the work function.

I identify three temperature regions:

i) $T < 500$ K, corresponding to spectra from n. 0 to n. 4;

ii) $500\ K \leq T \leq 600\ K$, corresponding to spectra from n. 5 to n. 8;

iii) $600\ K \leq T \leq 720\ K$, corresponding to spectra from n. 9 to n. 13.

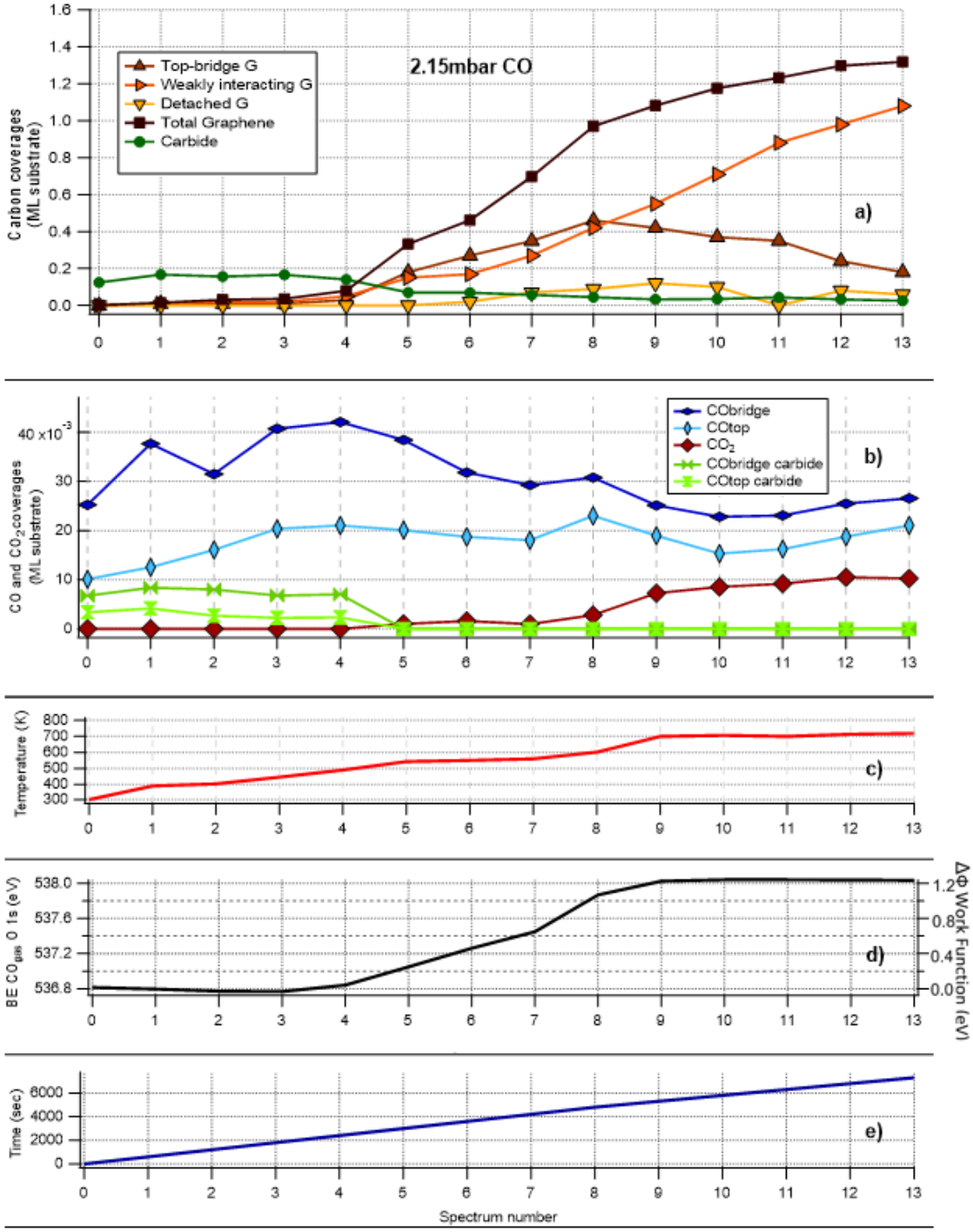

Figure 14 - a) Coverage of the different graphene components (top bridge (brown), weakly interacting (red), detached (gold) and total (black)) and of nickel carbide (green) with respect to the substrate. b) CO top, CO bridge and CO_2 coverage; c) Sample temperature; d) O 1s BE of CO_{gas} (the shift is proportional to the negative of the work function change of the surface); e) Exposure time. All data are derived from XPS spectra recorded at P_{CO} = 2.15 mbar.

Initially, the graphene coverage is still limited, and the only sizeable effect I observe is the increase of CO coverage. The latter is thereby estimated between 0.08 ML and 0.10 ML. I note that a comparable photoemission intensity for CO and carbide as in the present experiment were reported for Ni(110) (Monachino 2014) at 420 K and P_{CO} = 0.03 mbar.

The evolution of the system becomes more complex for 500 K ≤ T ≤ 600 K:

a) Graphene starts to grow effectively while the carbide coverage decreases. A similar amount of weakly interacting and of top-bridge graphene is now present at the surface, while detached graphene shows up only as a minor component.
b) CO adsorbed on carbide disappears completely while the coverage of bridge-bonded CO on Ni (now partly intercalated under the graphene cover) decreases and that of CO at on-top sites remains nearly constant. I note that the ratio between the intensity of intercalated CO and that of the graphene species is comparable with the one reported for a fully detached graphene layer (Wei 2015) indicating comparable coverage in these experiments. The absolute coverage calibration can, however, be affected by several factors such as the attenuation of the CO signal due to the graphene cover and the coexistence of interacting and noninteracting graphene domains. The local coverage could indeed be higher than the one I report due to the attenuation of the signal due to intercalated CO. At variance with Wei et al. (Wei 2015), however, no total detachment of the graphene layer from the substrate occurs. This finding indicates that CO intercalation is heavily influenced by the initial conditions, notably by the carbide covered fraction of the surface.
c) The work function decreases significantly upon graphene formation. For 600 K ≤ T ≤ 720 K, the relative amount of weakly interacting graphene increases at the expense of the top-bridge species, the CO coverage remains approximately constant and signal corresponding to physisorbed CO_2 intercalated under graphene appears. I note that weakly and strongly interacting graphene show similar growth rate and concentration as long as the physisorbed CO_2 signal is negligible, while the fraction of weakly interacting graphene becomes dominant when CO_2 starts forming under the graphene cover.

Notably, the work function decreases by 1.2 eV with respect to the initial condition. This change compares reasonably well with the difference in the work function between Ni(111) (5.5 eV) and graphene covered Ni(111) (4.25 eV), as estimated theoretically in ref. (Achilli 2018).

The shape of the Ni $2p_{3/2}$ line does not change appreciably upon graphene growth and exhibits only a tiny (0.2 eV) down-shift, thus allowing to exclude both oxidation of the substrate and formation of carbonates.

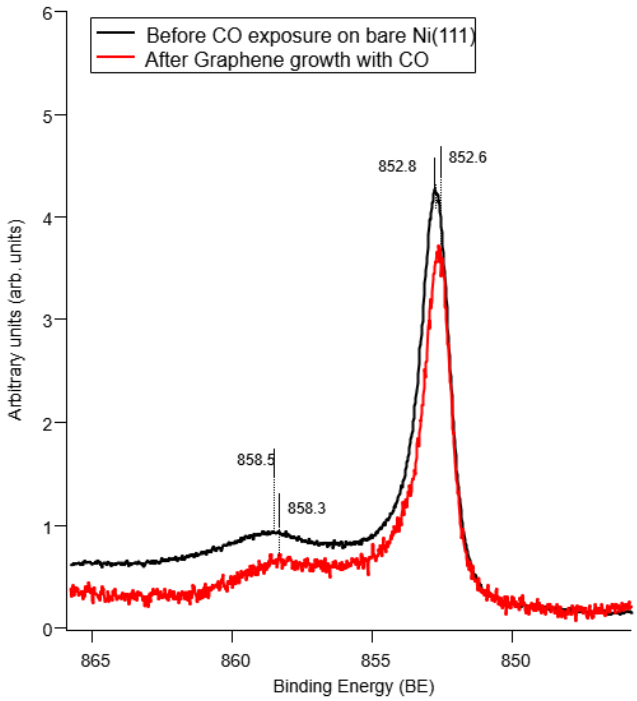

Figure 15 - Ni 2p3/2 line recorded at hv=970 eV before (black) and after (red) graphene growth by exposure to CO.

A Low Energy Electron Diffraction (LEED) and/or Scanning Tunneling Microscopy analysis would be valuable to provide structural information on the modifications of the G/Ni(111) system under CO pressure. While LEED inspection was not available on the experimental apparatus I used at the beamline, I mention that Perilli et al. (Perilli 2020) reported a LEED pattern with the same extra spots as for CO/Ni(111) upon CO intercalation at 0.5 mbar.

Finally, it is not obvious from the data whether the growth of graphene below 550 K is due to CO dissociation or to carbon formation via the Boudouard reaction catalysed by the Nickel surface. The observation of intercalated CO_2 proves, indeed, that the Boudouard reaction is effective at least above 600 K but it remains unclear whether CO_2 forms also at lower temperatures or not: if CO_2 formed already before graphene covers a significant fraction of the surface it could indeed move to the gas phase thus preventing its observation by XPS. Unfortunately, since it was not possible to measure the rest gas concentration during the experiment this question cannot be unambiguously answered on the basis of the available data. However, at variance with the experiment of Monachino et al. (Monachino 2014) we found no signal of adsorbed oxygen nor of surface oxide, thus suggesting that the Boudouard reaction contributes significantly to the growth of graphene also in the initial stages. These results should not surprise since dissociation of CO is expected to be less effective for Ni(111) than for Ni(110) (Monachino 2014) and because the higher pressure of CO of the present experiment makes the Boudouard reaction more likely to occur under the present conditions.

Whatever the reaction mechanism, my investigation proves that it is possible to grow graphene on Ni(111) by exposure to CO under NAP conditions at 550 K. As apparent from Table 2, this temperature is significantly lower than the one required for the growth of graphene on Ni using hydrocarbons since no dehydrogenation is required.

Table 2 - Comparison of the temperature required for the growth of graphene on Ni using CO and selected hydrocarbons.

Reactant	**Pressure (mbar)**	**(Minimal/reported) substrate Temperature (K)**	**Reference**
CO	2	550	This work
C_2H_4	$2\ 10^{-7}$ - $2\ 10^{-6}$	673-873	20
C_2H_2	$2\ 10^{-7}$	723-873	34
C_3H_6	$2\ 10^{-7}$	900	35
CH4 & H2	$2\ 10^{-7}$	1173	19

5. CO NAP exposure on graphene grown by CVD on Ni(111)

I report here an experiment in which I studied the interaction of graphene on Ni(111) by exposure to CO under near ambient pressure (NAP) conditions and I observed the occurrence of the Boudouard reaction. Despite the importance of this process in catalysis for coking as well as for growth of carbon nanotubes, at the best of my knowledge, this work is the first report in which the reaction is studied under controlled conditions.

The data relative to CO exposure on graphene-covered Ni(111) are shown in Fig. 16. The spectra, corresponding to the C 1s (left panel) and O 1s (right panel) regions, respectively, were recorded before and during exposure to CO. During the experiment the pressure has been set at 3.7 mbar and decreased only slightly (10%) during the experiment.

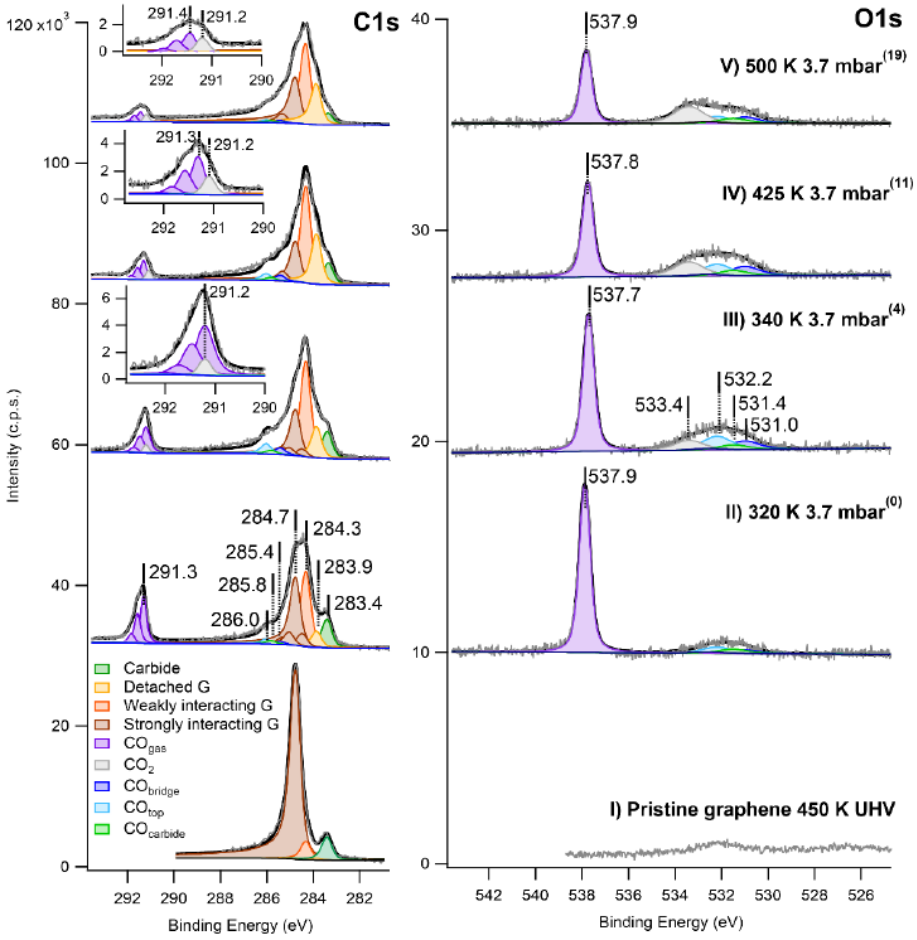

Figure 16 - NAP-XPS spectra of the C 1s (left) and O 1s (right) regions recorded for G/Ni(111) under UHV (bottom spectra) conditions and under P_{CO}=3.7 mbar. hv=650 eV for all spectra except for the C 1s region recorded under UHV, for which hv=400 eV. The spectra are presented without normalization and upshifted for the sake of clarity. Note the different scale in the panels of the two regions. All components contributing to strongly interacting graphene (top-fcc, top bridge and the minor contribution due to top hcp) are evidenced by brown filling. The small signal present around 532.0 eV before

intercalation is most likely due to traces of OH. Note that the photoemission intensity is strongly attenuated after the introduction of CO in the chamber so that the absolute intensities in UHV and after introducing CO cannot be directly compared.

It is apparent that:

a) Before introducing CO into the experimental chamber, oxygen is present only in trace amounts on the sample (see lower panel in Fig.16, the signal corresponds at most to 0.02 ML). The C 1s region shows features related mainly to strongly interacting graphene at 284.7 eV and to Ni_2C at 283.4 eV with only a minor contribution due to weakly interacting graphene at 284.3 eV.

b) The spectra are significantly modified by the exposure to 3.7 mbar of CO. Indeed, peaks due to gas-phase CO appear in O 1s and C 1s regions around 537.9 eV and 291.3 eV, respectively. In addition, in the O 1s region, a broad structure due to the convolution of new peaks at 531.0 eV, 531.4 eV and 532.2 eV, forms already at 320 K. The corresponding C 1s spectrum shows a change in shape. It now contains components at 283.4 eV, 283.9 eV, 284.3 eV, 284.7 eV, 285.4 eV, 285.8 eV and 286 eV. The components at 283.9 eV and at 284.3 eV are due to detached and weakly interacting graphene, respectively (Perilli 2020; Wei 2015).

Following the refs. (Wei 2015; Davì 2021), I assign the O 1s features at 531.0 eV and 531.4 eV to bridge bonded CO intercalated under the graphene layer and to CO at Ni_2C patches, respectively. The corresponding C 1s peaks at 285.4 eV and 285.8 eV overlap with the tail of the intense graphene features. The O 1s component at 532.2 eV and its companion at 286.0 eV are assigned to atop CO. The alternative assignment of the 532.2 eV peak to OH contamination is ruled out by inspection of the NAP-XPS spectrum. Indeed, the presence of water in the gas-phase should then be evident at E_B(O 1s)=536.0 eV (Patel 2019), while the intensity in that spectral region is less than 1% of that of gas-phase CO. Water intercalation followed by dissociation is not possible at such low partial pressures.

Upon annealing above 340 K, weakly interacting graphene becomes dominant over the strongly interacting one and also the detached graphene component increases in intensity. In addition, a new feature grows at 533.4 eV and becomes prominent over the other O 1s components for T≥425 K. This species is accompanied by the appearance of C 1s intensity at 291.3 eV, which partly overlaps with the signal due to gas-phase CO. As in the previous chapter this component is assigned to physisorbed CO_2 (Davì 2021). Given its low adsorption energy, it must be trapped under the graphene cover in order not to desorb at the temperature of the present experiment. The presence of this peak indicates that the Boudouard reaction is ignited.

The analysis of the data presented in Fig. 16 has been performed for all spectra of the series. The outcome is summarized in Fig. 17 vs spectrum number and discussed in the following. The spectra were recorded sequentially at nearly constant CO pressure (~3.7 mbar) while increasing the crystal temperature (see panel E of Fig. 17).

Panel A shows the evolution of the graphene, carbide and total carbon coverage while the fractional area covered by the different graphene species and by carbide is reported in panel B. Panel C shows the CO and CO_2 coverage obtained assuming that the molecules are intercalated below the graphene sheet. The atop CO peak results from the unresolved contributions of intercalated CO at Ni sites and of weakly bonded CO adsorbed at graphene sites, which is not screened by the graphene layer. Since for all species the coverage has been corrected for the attenuation of the G cover (roughly a factor of 2.3), the amount of weakly adsorbed CO on graphene reported in the figure is overestimated by the same factor.

Lastly, the work function change is reported in panel D. I mention that the work function value, ϕ, for G/Ni(111) is still controversial; values reported in the literature differ significantly, ranging from 3.66 eV (Weatherup 2011) to 4.25 eV (Achilli 2018), but they are always lower than the one of 4.48 eV of free-standing graphene (Giovannetti 2008). In our experiment, $\Delta\phi$ increases up to spectrum 3, decreasing eventually slowly starting from spectrum 7. This behavior results from the combined effects of the graphene detachment due to CO intercalation and of the presence of weakly adsorbed CO above graphene, as it will be discussed in the following.

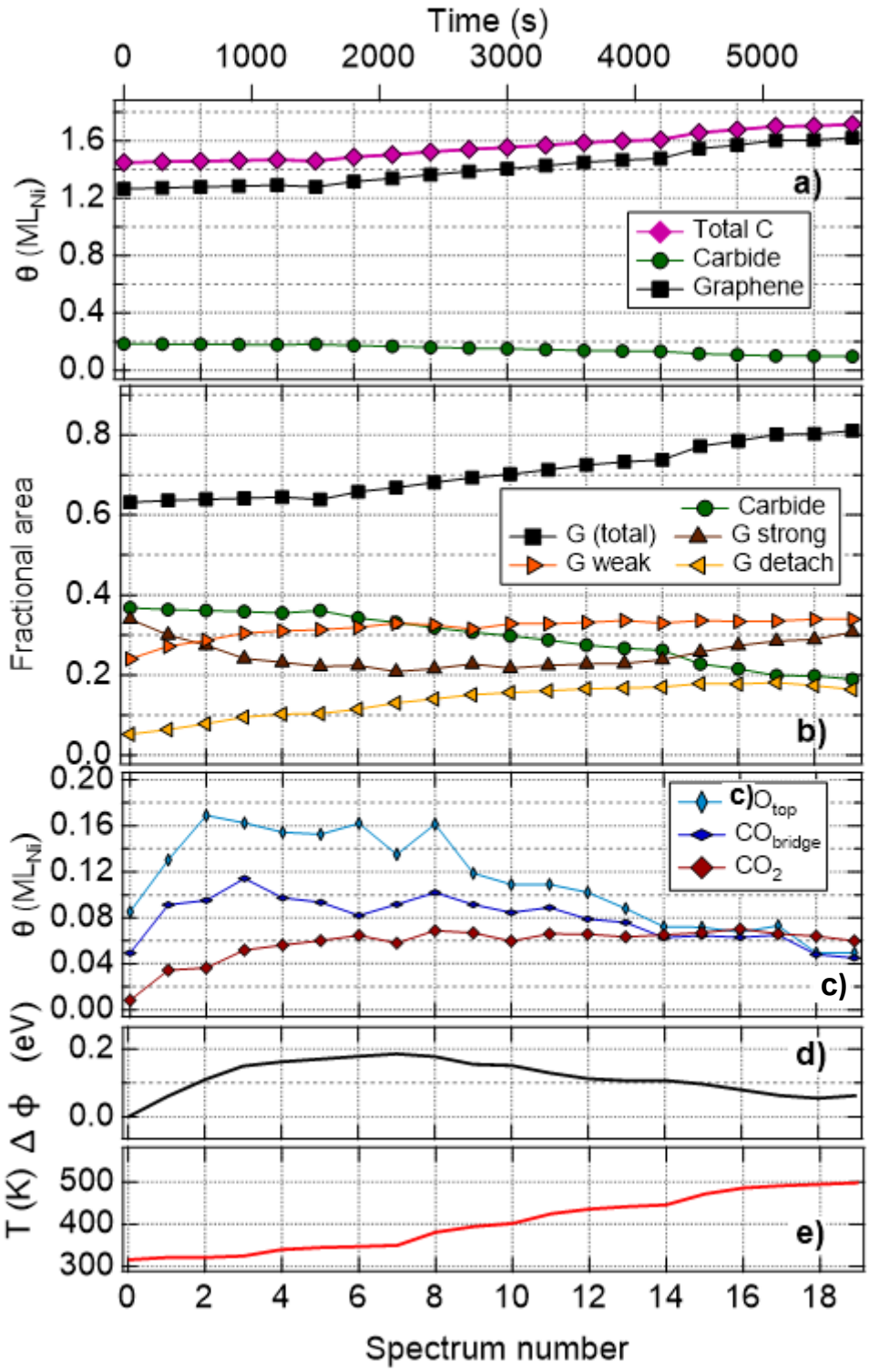

Figure 17 - Analysis of the data reported in Fig. 1. The abscissa refers to the number of subsequent spectra recorded in the experimental run. a) Carbon coverage of graphene and carbide. The total carbon coverage is also reported. b) Fractional area of the different graphene species and of carbide. For the procedure followed to calculate these fractional areas I refer to the experimental section). It assumes that the surface is entirely covered by either graphene or carbide. c) Coverage of CO at atop and bridge sites and of CO_2. d) Variation of the average work function $\Delta\phi$. e) Variation of the temperature of the sample vs spectrum number.

I note that, already from the first spectra, the surface fraction covered by strongly interacting graphene (E_b=284.7 eV) decreases and only partially recovers at the highest temperature (panel B). In literature (Africh 2016; Wei 2015) the carbon- containing species with C 1s~284.4 eV is ascribed to weakly interacting graphene. Such component (at E_b=284.3 eV in the present case) and the detached (E_b=283.9 eV) graphene initially increase and then remain stable.

Africh et al. identified weakly interaction graphene with rotated graphene domains sitting above carbide-covered areas (Africh 2016); alternatively, it might correspond to the second layer of bilayer graphene patches. Neither explanation seems to be appropriate to describe the current results. The scenario with weakly interacting G sitting above carbide is ruled out since the amount of carbide is very small or even missing for a G layer grown by C_2H_4 dehydrogenation. Moreover, weakly interacting G appears promptly upon CO intercalation and grows together with the detached graphene component with E_B(C 1s)=283.9 eV, while carbide coverage decreases. The assignment to a second graphene layer is also unlikely since, if it was the case, the intensity of the strongly interacting G component should keep more or less constant, contrary to the experimental outcome. My data suggests therefore that CO intercalation proceeds from the edges of graphene flakes and reaction occurs far away from the borders causing the formation of graphene bubbles in which detached graphene is at the center and weakly interacting graphene (displaying an intermediate E_B value in-between those of detached and strongly interacting graphene) sits at the borders.

Under CO pressure, the total carbon coverage increases with increasing temperature by about 0.25 ML (see panel A of Fig. 17). This increase corresponds due to the growth of the fractional area covered by graphene at the expense of the one covered by carbide. The carbide carbon content (estimated as ~ 0.09 ML) is not sufficient to account for this change.

However, formation of CO_2, occurring already at 340 K (panel C of Fig. 17) and indicative of the onset of the Boudouard reaction, can account at least for part the additional carbon. Indeed, the amount of CO_2 is estimated to ~0.05 ML. We note, on one side, that it is not possible to expect a quantitative accord due to the difficulties in the absolute coverage calibration of the adsorbed species and, on the other side, because the observed CO_2 signal might correspond to the equilibrium coverage between CO_2 production and deintercalation. The carbon production by the Boudouard reaction could thus be underestimated. This hypothesis is supported by the fact that the CO_2 signal promptly decreases upon evacuation of the experimental chamber hosting the sample (see Fig. 22 below).

According to literature, the E_B of gas-phase CO_2 is expected around 537.0 eV and 293.6 eV in the O 1s and C 1s regions, respectively (Blomberg 2013; Avval et al. 2019). A small signal at that binding

energy is indeed sometimes present in the C 1s region (not shown) but the corresponding O 1s peak must be more heavily damped than the C 1s signal because it is not evident in the spectra. Since the noise level is typically 4% of the O 1s intensity for gas-phase CO, we conclude that the partial pressure of gas-phase CO_2 cannot exceed 0.15 mbar, implying that the Boudouard reaction rate is lower than 4% under the present conditions. Such reactivity is, however, sufficient to generate the detected coverage of physisorbed CO_2 under the graphene cover and to provide the required amount of carbon.

Possible alternative C sources are excluded for the following reasons: Firstly, the absence of atomic oxygen or nickel oxide signals in the O 1s spectrum rules out that additional carbon is generated by CO dissociation at defects of the substrate. Indeed, given the high CO pressure, the oxygen released by such process could be efficiently removed by reaction with further CO. However, CO oxidation on Ni(111) occurs only at high atomic oxygen coverage, while it is endothermic at low oxygen coverage (Avval 2019). At 1/3 ML the reaction has an activation barrier of 0.83 eV (Peng 2010), while low-temperature oxidation is possible in the presence of weakly bonded atomic oxygen. Secondly, the hypothesis that carbon is provided by segregation from the bulk is also inconsistent since the growth of graphene by this mechanism does not take place below 580 K (see discussion of Fig. 11, cap. 4). We can thus safely conclude that the formation of the additional carbon is due to the Boudouard reaction.

Fig. 17 c) shows that the coverage of CO molecules adsorbed both at top and bridge sites (CO_{top} and CO_{bridge}, respectively) increases rapidly upon CO exposure and decreases eventually with rising temperature. CO_{top} is initially more abundant but at the highest T the coverage of the two species becomes comparable. On the contrary, the CO coverage increases when the sample is cooled to 320 K, under which conditions the top species dominates over the bridge one (see Fig. 18,19).

To rationalize this complex behaviour we have to recall that both intercalated CO adsorbed at Ni(111) top sites and on-surface CO adsorbed at G top sites contribute intensity at E_B~286.0 eV. Even if they cannot be directly resolved in the XPS spectra, they are characterized by a different thermal stability. To estimate the different contributions of intercalated and on-surface CO to the CO_{top} coverage, we start considering the equilibrium coverage vs sample temperature for CO adsorbed on bare Ni(111) (Fig. 18, black curve) and on G/Ni(111) (purple curve) at a CO pressure of 3 mbar. The curves are calculated from calorimetric data for CO on Ni(111) using a parabolic interpolation.

For weakly adsorbed CO on G/Ni(111) a linear dependence was assumed for the adsorption energy with the initial value and the slope estimated in ref. (Smerieri 2015). It is apparent that desorption of CO weakly adsorbed on graphene must occur at a much lower temperature than de-intercalation

of CO bound to Ni(111). The decrease of the CO_{top} intensity observed in Fig.17 c) must then arise mainly from the desorption of the weakly adsorbed moiety.

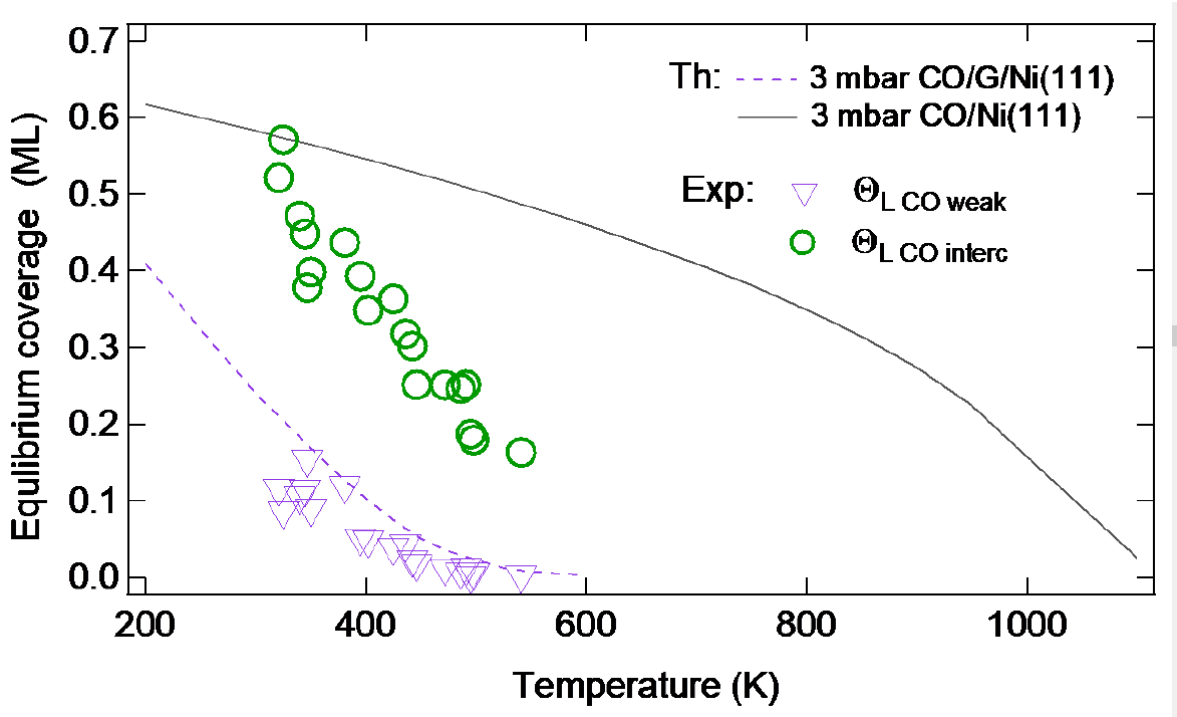

Figure 18 - Estimated equilibrium coverage of CO on Ni(111) (using the calorimetric data of ref.(Stuckless et al. 1993) *– black curve) and for weakly adsorbed CO on G/Ni(111) (purple dashed curve*(Smerieri et al. 2015)*). The calculations are compared with the local CO coverage observed for the weakly bonded (CO_{weak}) species on graphene and the intercalated (CO_{interc}) one.*

The variation of Δϕ with sample temperature during the experiment (see Fig.17 d)) supports this conclusion. In fact, its initial increase can be explained both by the adsorption of CO on graphene and by the detachment of graphene due to CO intercalation since effects induce a change with the same sign. The slow decrease observed after scan 7, on the contrary, is unexpected in view that in this temperature range the relative amount of weakly and detached graphene increases and the one of strongly interacting graphene remains nearly constant. Therefore, the observed behaviour can be rationalized only by the desorption of weakly adsorbed CO *above* graphene.

At 500 K only intercalated CO is stable. In this condition we observe a comparable signal for atop and bridge bonded CO. This result is at variance with literature for the same system (Del Puppo 2021; Wei 2015) and for CO on bare Ni(111) (Held 1998), for which bridge CO is dominant. However, on bare Ni(111), a comparable population of CO at top and bridge sites was reported by Infrared Reflection Absorption Spectroscopy for the compressed 0.57 ML phase obtained in UHV at 80 K (Trenary 1985). On the contrary, little or no CO at top sites is detected experimentally for G-covered Ni(111) (Del Puppo 2021; Wei 2015) while *ab-initio* calculations predict that this species is not stable

under cover. At variance with the cited papers, our experiments were performed in-operando conditions, i.e. recording the XPS spectra in CO pressure and for RT≤T≤500 K.

Having already ruled out the possibility that the 532.2 eV signal is related to OH species, I tentatively explain the different outcome of the present study with the different experimental conditions. I also mention that the theoretical calculations excluding the presence of intercalated CO at top sites were performed for a fully detached graphene layer while, in our experiment, a mixed layer consisting of patches of strongly interacting, weakly interacting and detached graphene is present. The situation is therefore more complex, since the coverage of intercalated CO is not uniform and areas of high local coverage of intercalated CO coexist with areas where no intercalation has taken place and CO weakly adsorbs at RT under NAP conditions.

I conclude therefore that the total energy of such a mixed layer can be lower than the one of a fully-detached layer, with only bridge bonded CO. Indeed at high local coverage the adsorption energy of CO under G is calculated to be around -1.7 eV/molecule and has to be compared to -2.1 eV/eV molecule on bare Ni (Del Puppo 2021). The difference, which accounts for the cost of the detachment of the graphene layer is in fact comparable with the adsorption energy of weakly adsorbed CO above graphene, estimated experimentally to be around 0.35 eV/molecule at 1/3 ML coverage and even higher at lower coverage (Smerieri 2015). This gives a rational to the observation that no full delamination of the graphene layer occurs, despite the higher pressure with respect to the previous studies (Del Puppo 2021; Wei 2015) where full delamination was reported. Indeed, I also observe atop CO, which could be stable under graphene bubbles given the high local coverage.

Considering that intercalated CO can be present only under the detached or the weakly interacting graphene areas, which cover about half of the sample, I estimate a local CO coverage of ~0.5 ML (though it may be different under weakly and detached G areas), thus compatible, within the error, with the possibility of populating a compressed phase under dynamical equilibrium conditions in which both top and bridge sites are occupied in comparable amount, as it occurs in UHV on bare Ni(111) at low temperature (Trenary 1985).

To determine the fraction of non-intercalated atop CO, I assumed that under all conditions the coverage of atop and bridge CO under cover is comparable, as it is indeed the case at high temperature. The total coverage of intercalated CO ($\Theta_{COinterc}$) is then twice the one of bridge CO. The coverage of CO weakly adsorbed on graphene (Θ_{COweak}) and overlapping with intercalated CO at atop sites, can then be estimated from the difference between the intensity of atop and bridge

CO after removing the correction for the attenuation factor *fatt*~2.3 due to graphene, which should be applied only to the intercalated species. Since CO binds only to strongly interacting graphene (Smerieri 2015) the *local* coverage of CO weak ($\Theta_{L\,CO\,weak}$) can be obtained by dividing Θ_{CO} weak by the fractional area occupied by strongly interacting graphene. The resulting coverage is shown by the violet triangles in Fig. 17 which are indeed in nice agreement with the expected equilibrium value $\Theta_{LCOweak}$. Similarly, the *local* coverage of intercalated CO_{interc} ($\Theta_{L\,COinterc}$) may be estimated by dividing $\Theta_{COinterc}$ by the total fractional area occupied by weakly adsorbed plus detached graphene. It is apparent from Fig. 17 that $\Theta_{L\,COinterc}$ decreases with temperature more rapidly than expected for CO/Ni(111). This high desorption/deintercalation rate could indicate a partial conversion into CO_2 and/or a lower adsorption energy of CO under the graphene cover. Indeed, for the similar system CO/Pt(111) the adsorption energy decreases from 1.74 eV/molecule to 1.21 eV/molecule for the intercalated species (Yao 2010).
Note that if the amount of intercalated atop CO would be lower, the relative amount of weakly adsorbed CO would be even higher. A constraint on the maximum amount of weakly adsorbed CO is provided by the intensity of the 532.2 eV peak persisting upon evacuation of the chamber (see Fig. 23 below) which can only be due to intercalated CO at atop sites.

To reinforce the assignment to weakly bonded CO on G/Ni(111) of part of the signal at E_B(C 1s)=286.0 eV, we performed the additional experiment reported in Fig. 19. Starting from a G/Ni(111) sample with intercalated CO, we slowly decreased the temperature from 490 K to 313 K under nearly constant CO pressure. Under these conditions, normalization of the spectra to the background is possible, allowing for a direct comparison of the peak intensities. Upon cooling, the O 1s features related to adsorbed species increase in intensity while the main C 1s peak decreases and a shoulder grows on its high binding energy side. Both the C 1s and O 1s peaks related to gas-phase CO downshift with cooling, indicating an increase in the work function. Considering that in this sample temperature range the relative amount of strongly interacting, weakly interacting and detached graphene remains nearly constant, the work function variation can only be induced by CO adsorption at G/Ni(111). Since this is the only change taking place in the system, it must also be responsible for the enhanced asymmetry of the C 1s line of graphene.

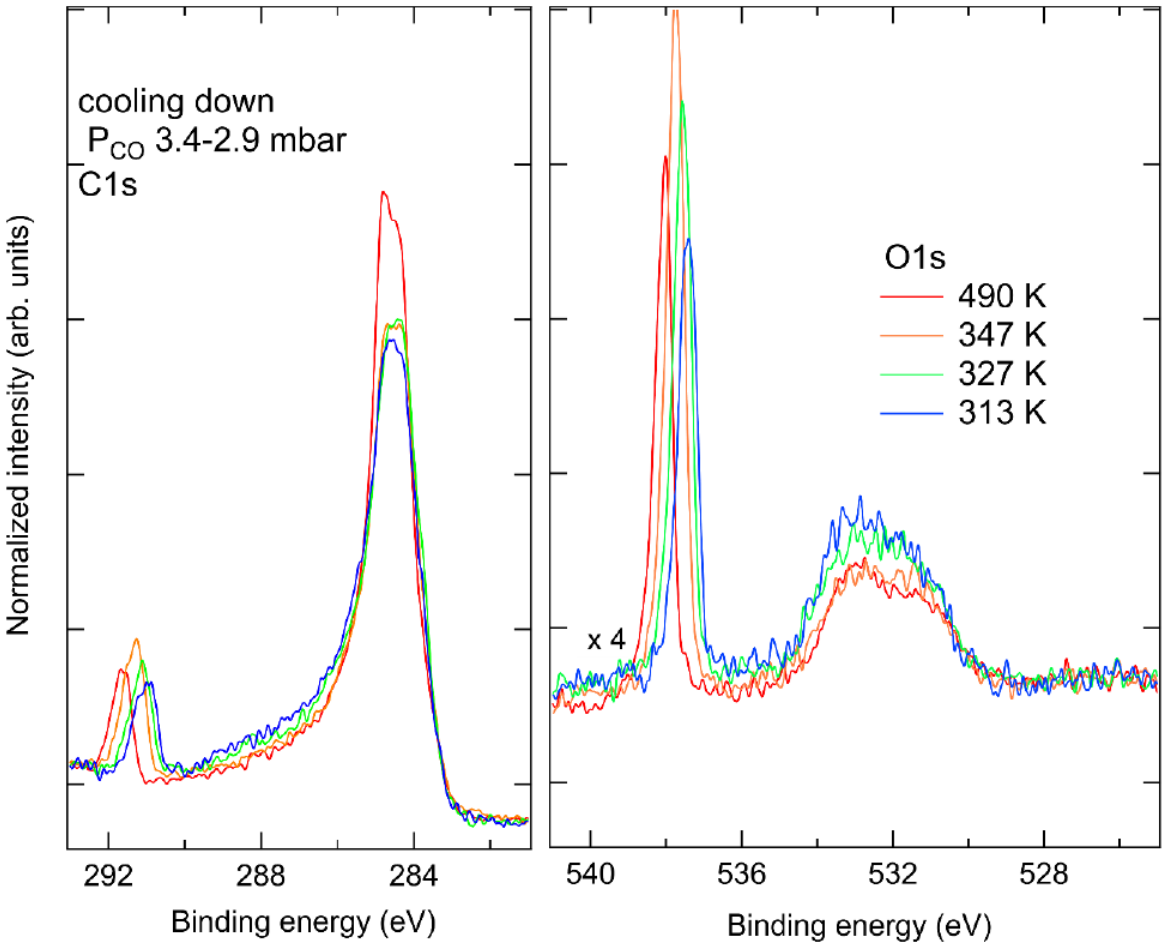

Figure 19 – C 1s (left) and O 1s (right) XPS spectra recorded while cooling the sample from 490 K to 313 K in P_{CO} ~ 3.1 mbar. The C 1s spectra are normalized to the area of the G-related peaks between 283.0 eV and 290.0 eV. O 1s spectra are normalized on the background and rescaled in order to maintain the stoichiometric C 1s/O 1s ratio (note the multiplication factor applied to the O 1s region for a better visualization).

In Fig. 20 are shown the spectra with the fitting used to calculate the coverages of the adsorbed species

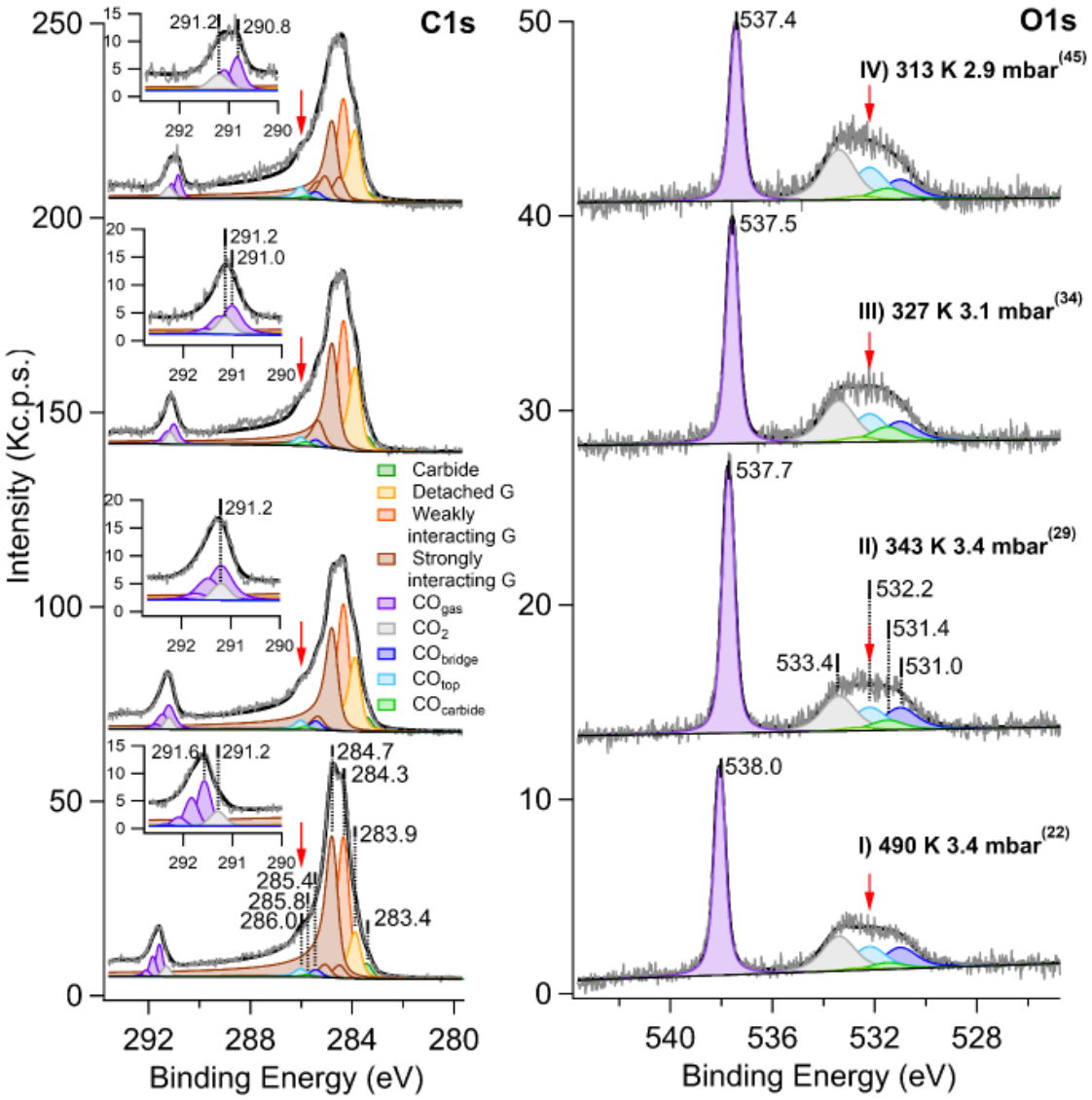

Figure 20 – Best fits of Fig.19; C 1s (left) and O 1s (right): I) 490 K, 3.4 mbar; II) 343 K, 3.4 mbar; III) 327 K, 3.1; IV) 313 K, 2.9 mbar the number within brackets refers to the spectrum number of Fig. 17.

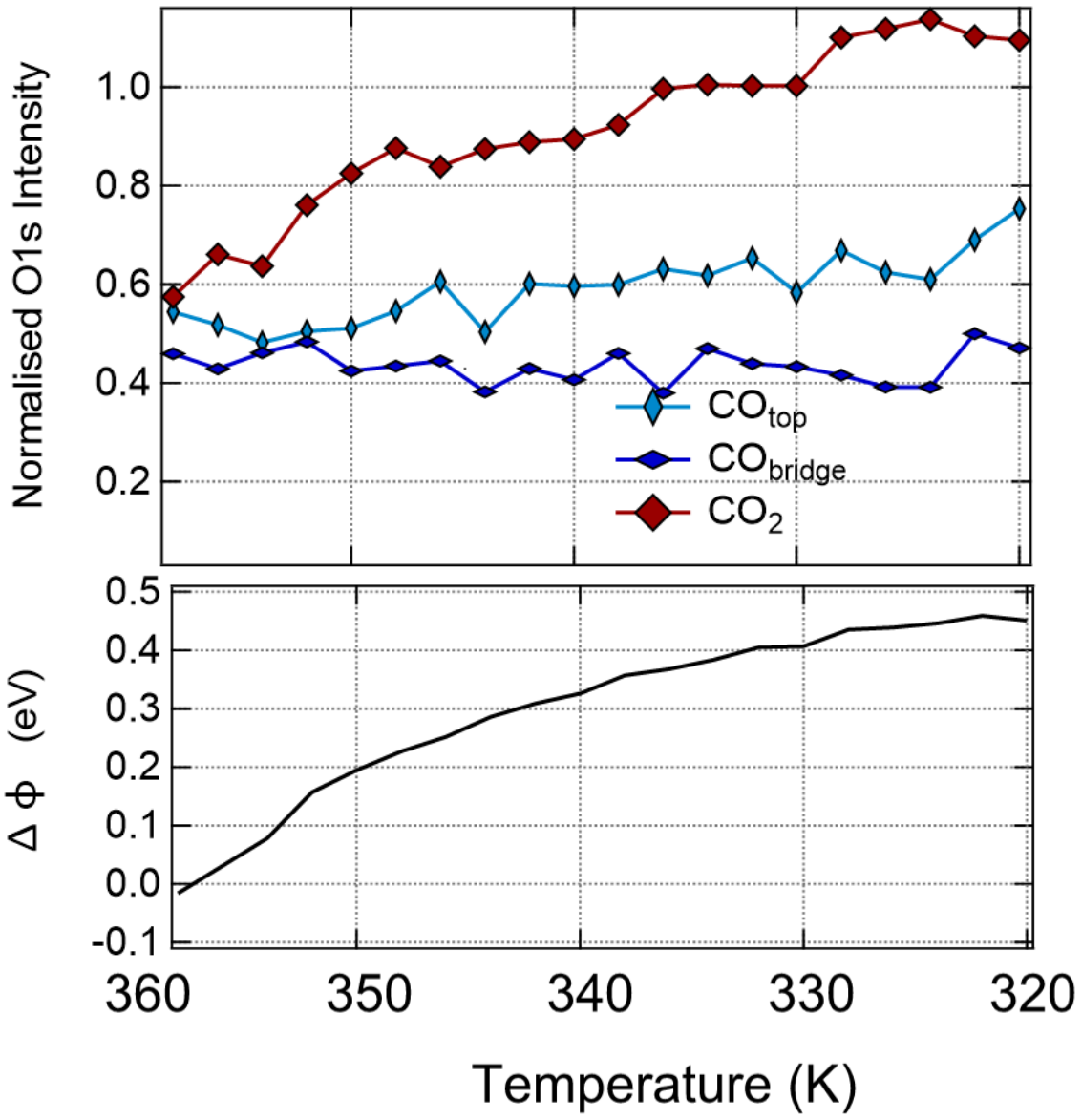

Figure 21 - Analysis of the series of spectra of Fig. 16 vs sample temperature. A): O 1s intensity of CO_{bridge} (blue lozenges), CO_{top} (light blue rhombuses) and CO_2 (red squares) normalized to the background. B) Work function variation. Note the decreasing values scale of the temperature, corresponding to the cooling process.

The intensities of the different CO species deduced from the fitting of the O 1s region (see Fig. 20) and normalized to the background and the work function changes are plotted in Fig. 20 vs sample temperature. While the CO_{top} intensity increases for T<340 K, that of CO_{bridge} remains nearly constant over the whole T range.

In addition, I note that the amount of physisorbed CO_2 under cover, corresponding to the O 1s component at 533.4 eV, grows almost linearly with decreasing T. This is in apparent contradiction with the fact that the CO_2 signal was also observed to increase while heating the sample. The overall

picture can be rationalized reminding that CO_2 formation needs a high concentration of intercalated CO, which is only possible after the detachment of a significant fraction of the graphene layer.

Therefore, the CO_2 signal observed in the annealing sequence results from the combination of two competing effects: the rate of the Boudouard reaction (decreasing with increasing T), and the area of detached and weakly interacting graphene (larger at higher T). When cooling down, on the contrary, the CO_2 signal is uniquely determined by the increase of the equilibrium constant of the Boudouard reaction since the catalytically active area (proportional to the amount of detached/weakly interacting graphene) remains constant.

Finally, any possible alternative assignments of the 533.4 eV line other than physisorbed CO_2 under cover is ruled out. In fact, the possibility that it may be due to transient water contamination does not hold since, given the low adsorption energy of water, a significant partial pressure in the gas-phase would be needed to justify a metastable coverage resulting in such intensity and the O 1s line of gas-phase H_2O would be expected around 536 eV,(Patel et al. 2019) but no such contribution is present in the experimental spectra.

I can also exclude that the peak is due to the formation of tetracarbonyl-nickel since the corresponding feature is missing in the Ni 2p spectrum at least within our experimental sensitivity. Such a signal would indeed be expected given the cross-section for Ni 2p at 970 eV photons and the one for O 1s at 650 eV. Moreover, the formation of tetracarbonyl-nickel is expected to be thermodynamically less favoured than the Boudouard reaction because it involves four CO molecules instead of two.

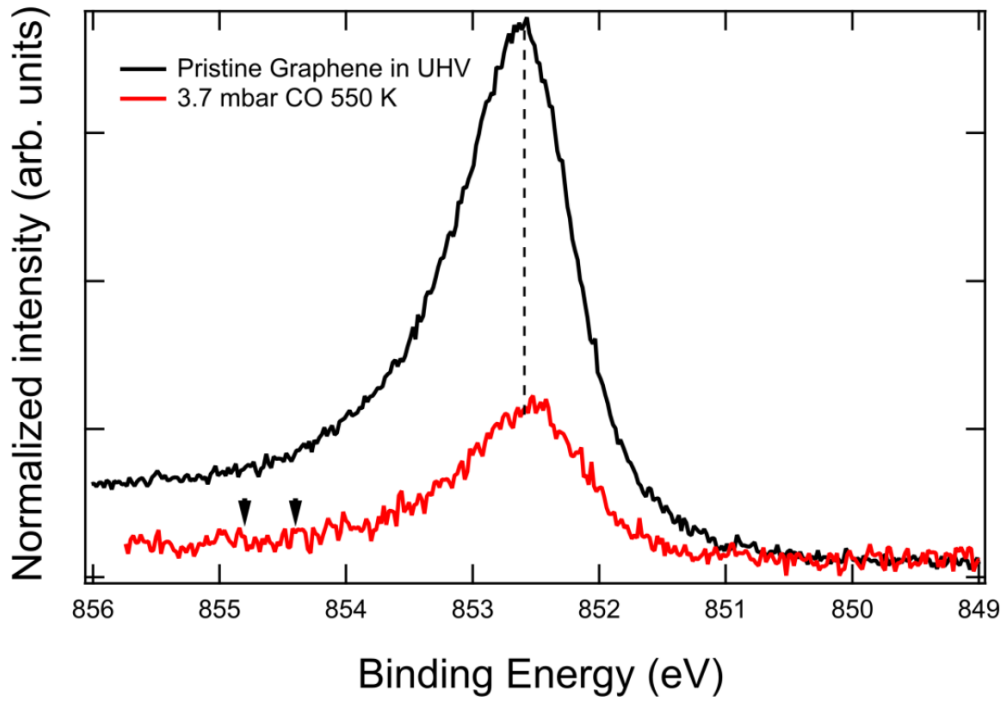

Figure 22 - Normalized Ni 2p spectra recorded for pristine graphene in UHV and under a pressure of 3.7 mbar of CO. The photon energy is 970 eV. The arrows indicate the position of the Ni 2p line expected for tetracarbonylnickel ($Ni(CO)_4$) according to(Africh 2016).

The signal at 533.4 eV disappears when the system is evacuated (see Fig. 22). A direct comparison of the spectra under NAP and UHV conditions is not possible because of the already mentioned attenuation of the signal due to gas-phase CO. To compare the spectra of Fig. 22 I proceeded, therefore, as follows:

1) i assume that the graphene sheet is not affected by the evacuation process. The attenuation of its XPS signal allows then to determine the distance, d, between the sample and the nozzle by $I_{(pCO)}=I_{UHV}\ exp^{(-d/\lambda C1s)}$, where I_{UHV} and $I_{(pCO)}$ are the intensity in the absence and in presence of the background pressure, p_{CO}, respectively. The mean free path of C 1s electrons, $б_{C\ 1s}$, is then calculated from the CO gas density and the cross-section for inelastic scattering of electrons having the kinetic energy of C 1s photoelectrons in our experiment (taken from ref. (Itikawa 2002) as the difference between the total cross-section and the elastic cross-section).

2) A similar relationship is used to estimate the attenuation of the signal due to O 1s electrons using the corresponding $б_{O1s}$ and the distance d.

3) The so-obtained correction factors for the C 1s and O 1s lines are used to rescale the corresponding spectra after subtraction of a linear background.

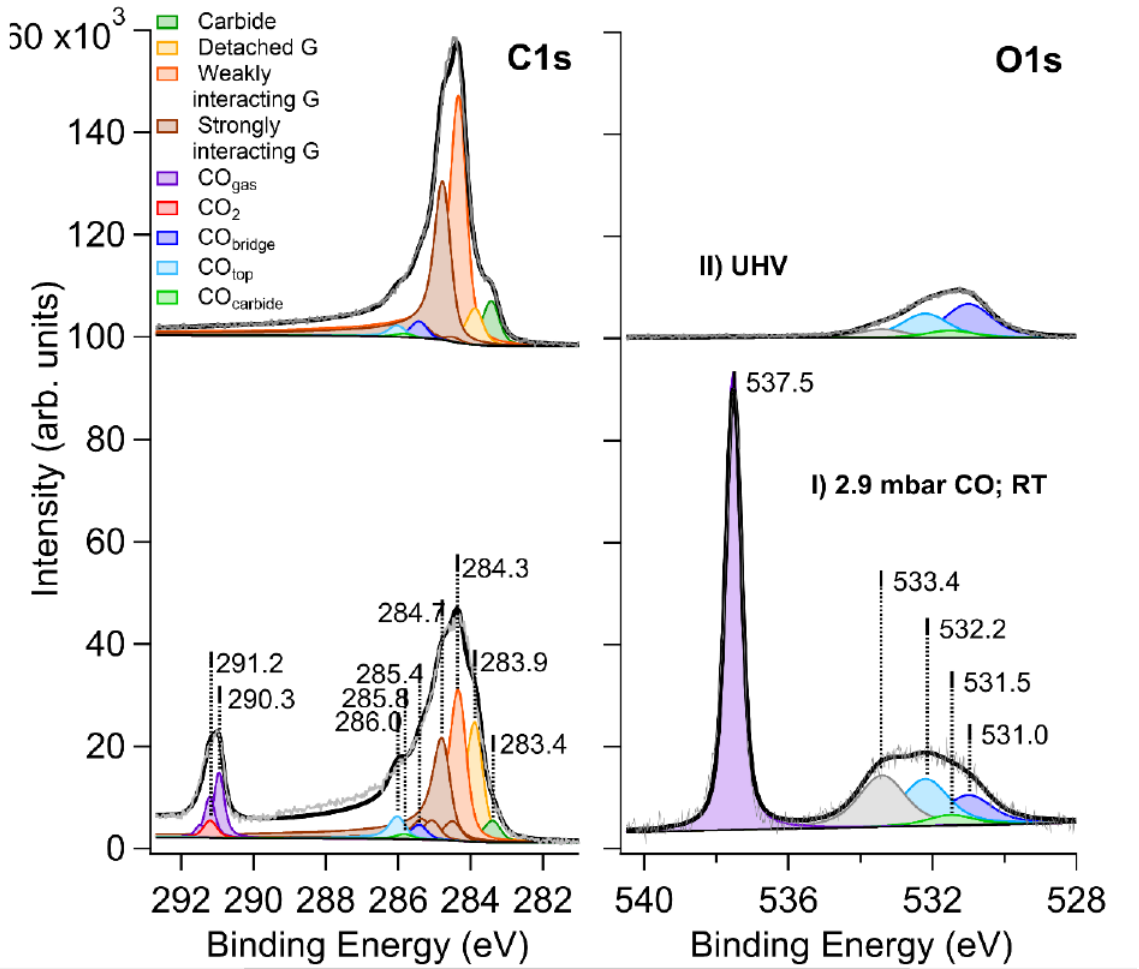

Figure 23 - Comparison of the XPS spectra of G/Ni(111) at T=313 K before (bottom, p_{CO}=2.9 mbar) and after (top, UHV) evacuating the experimental chamber. The spectra of the C 1s and of the O 1s region have been corrected for the attenuation due to the gas-phase (see text).

To better evidence the differences before and after CO evacuation, in Fig. 23, I report the overlapped spectra with no fitting:

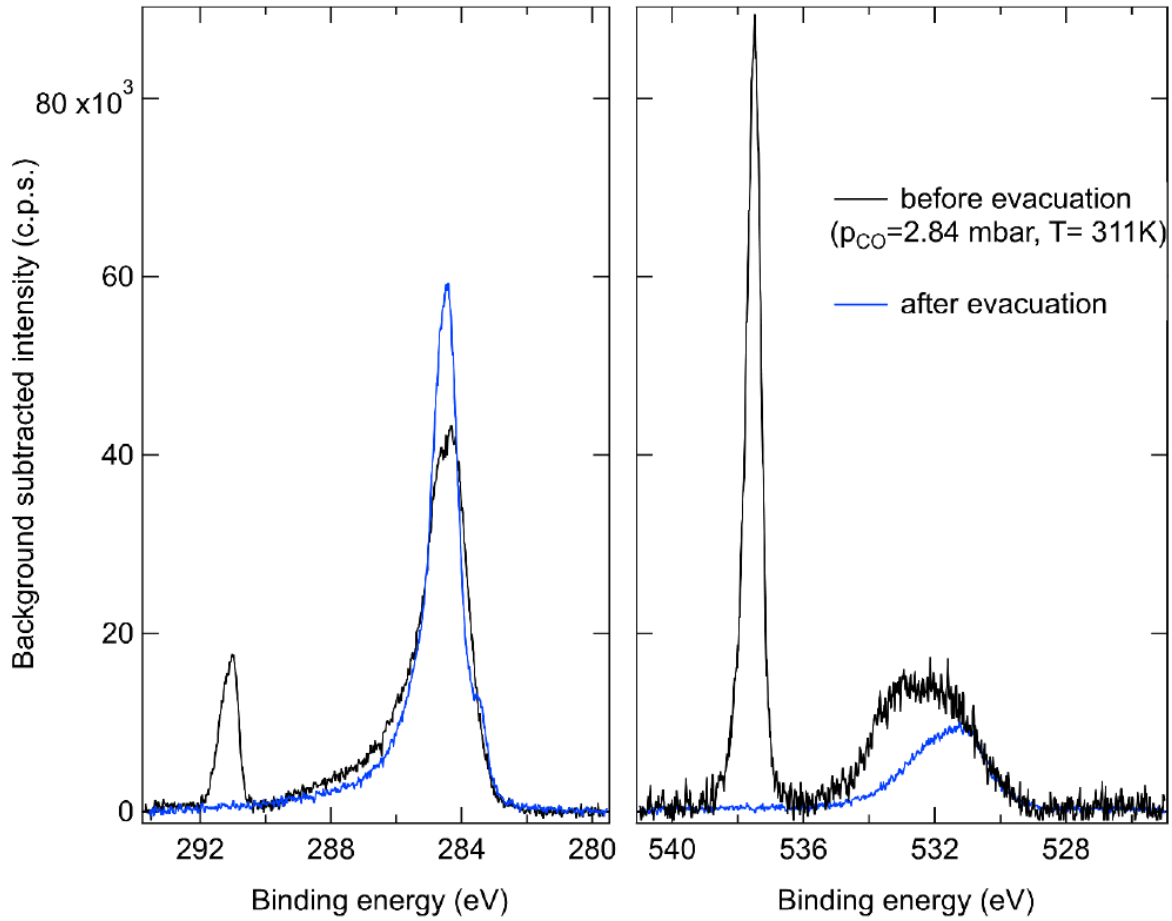

Figure 24 – direct comparison of the spectra of figure 22.

Upon evacuation of the experimental chamber (see Fig. 22) both the asymmetry and the O 1s components due to CO_2 and to the weakly adsorbed CO species have disappeared. The final intensity of the 532.2 eV component is now smaller than the 531.0 eV component, due to bridge bonded CO, which remains almost unaffected. Such behavior indicates that:

i) intercalated bridge-bonded CO is stable at room temperature;

ii) since the intensity of atop-CO and bridge-bonded CO are expected to be equal under CO pressure at RT, the fact that the 532.2 eV component is now smaller indicates that part of intercalated atop-CO was metastable and has now de-intercalated. This is coherent with the lower adsorption energy expected for this species.

The narrowing of the graphene peak is thereby associated with the decrease of the weakly interacting and detached components.

6. CO NAP exposure on graphene on NI(111) defected by sputtering

The aim of the present experiment is to functionalize the graphene layer by drilling isolated holes in it by sputtering. The latter procedure took place by filling the chamber to a pressure of 10^{-6} mbar of Ar, ionizing it and applying a bias of 150 V to accelerate the Argon ions towards the sample for a sputtering time of 60 sec. According to previous experimental (Ugeda 2011, 2012) and theoretical (Lehtinen 2010) studies, Ne^{+} irradiation under very similar conditions produces single and double vacancies (*i.e.* situations in which only one C atom or two adjacent C atoms of the G lattice are removed, respectively) in $\sim 5:2$ ratio.

Unfortunately, it was not possible to read out the sample current to determine the sputtering yield, but an estimate of the density of defected carbon sites can be obtained by the decrease of the strongly interacting component of the graphene layer caused by the sputtering action. After the sputtering procedure approximatively 5% of the carbon intensity has disappeared due to the sputtering action.

The spectra recorded before and after the sputtering procedure are shown in Fig. 25.

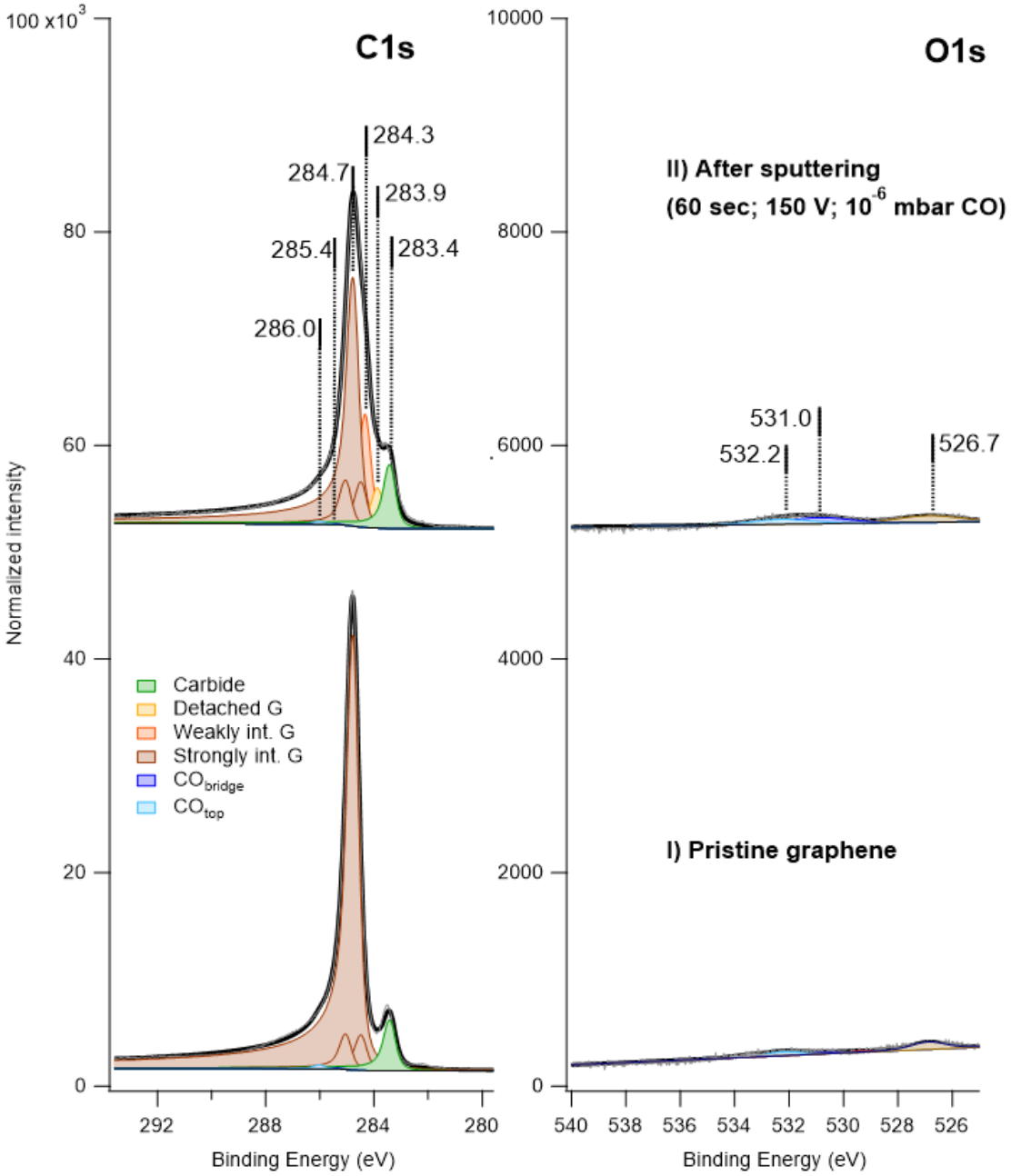

Figure 25 – NAP-XPS spectra of the C1s (left) and O1s (right) regions for G/Ni(111) of the graphene layer as grown (bottom spectra) and after the sputtering action (top spectra). hv=650 eV for all spectra. The spectra are normalized to the background at low binding energies.

In Fig 24 1) I show the spectra obtained for a system grown following the procedure discussed in chapter 3. As in the previous experiment, in the C 1s region, the strongly interacting graphene component is initially dominant, indicating that this species covers most of the surface. Carbide is present only as a minority species. In the O 1s region, the adsorbed CO features and a component due to an unknown contaminant at 526.7 eV are present in negligible amounts. No change occurs in the O 1s region. In particular, no significant increase of the adsorbed CO species takes place and,

since the CO sticking coefficient to Ni(111) is very high, I can conclude that no bare Nickel areas have been exposed. I also observe the transformation of 35% of the strongly interacting graphene either into carbide or into other carbon species with slightly lower binding energies (from 283.7 eV to 284.3 eV) than the strongly interacting graphene one.

In the above mentioned energy window, it is possible to assign some components to species expected to form due to the sputtering treatment such as: dissolved carbon at 283.7 eV (Smerieri 2015); detached graphene at 283.9 eV; weakly interacting graphene at 284.3 eV; carbon atoms at the border of the holes which form bonds with the underlying Nickel atoms. Due to the multiplicity of the species and the closeness of the corresponding E_B values, it is not straightforward to separate these components. I decided therefore to fit the intensity from 283.7 eV to 284.3 eV with two components marked as "weakly interacting" and "detached graphene" (Fu 2017). Such components are indeed predominant in the spectra recorded after dosing CO.

As already discussed in the previous chapters, in order to determine the O 1s and C 1s intensities due to the oxygen containing species consistently, I have to consider the effect of the attenuation of the photoemission intensity due to the presence of the gas phase molecules.

To this purpose, I firstly determine the intensity of the different O 1s components and fit eventually the C 1s region by assigning the corresponding C 1s intensity in two different ways depending on the pressure range:

1) Under UHV conditions the intensity ratio between O 1s and C 1s component is determined by the corresponding photoemission cross-sections ($б_{C1s}$=1.5 Mb; $б_{O1s}$=3.5 Mb at 650 eV), the transmission function of the analyzer being constant over the scanned energy interval, and by the stoichiometry of the species.

2) Under NAP conditions (already described in chapter 3.2 and reported here for clarity), the photoemission intensity is affected by the electron kinetic energy dependent attenuation of the signal due to scattering off gas-phase molecules. $I_{C1s\ ads}$, must then satisfy the relationship of Equation 5 of chapter 3.2, i.e.:

$$I_{O1s\ ads} / I_{O1s\ COgas} = \varepsilon\ I_{C1s\ ads} / I_{C1s\ COgas}.$$

where the stoichiometry is ε=1 for CO and ε=2 for CO_2, $I_{O1s\ ads}$ is the intensity of the O_{1s} line of the adsorbed moiety and $I_{O1s\ gas}$ and $I_{C1s\ gas}$ are the intensities of the corresponding gas-phase CO lines. It is clear that the first method is adequate in UHV conditions while the second is justified at pressures higher than 1 mbar.

In this experiment, however, the spectra have been acquired also in an intermediate pressure region (10^{-1} mbar 10^{-2} mbar). In order to consolidate the validity of our assumptions in such range, I calculated the expected intensities following both methods.

Fig. 26 can ideally be divided into three regions: the first (from spectrum n^{o} 0 to spectrum n^{o} 8) in which I report only the intensities calculated with the first method due to a lack of gaseous peak; the second region (from spectrum n^{o} 9 to spectrum n^{o} 13) between 10^{-1} mbar and 10^{-2} mbar in which I observe that the matching between the two procedures is acceptable and thus our calculation can be trusted also in this range; the third region (from spectrum n^{o} 14 to spectrum n^{o} 35) in which the intensities calculated with the two different calculations differ by a factor of approximatively two but maintain the same trend.

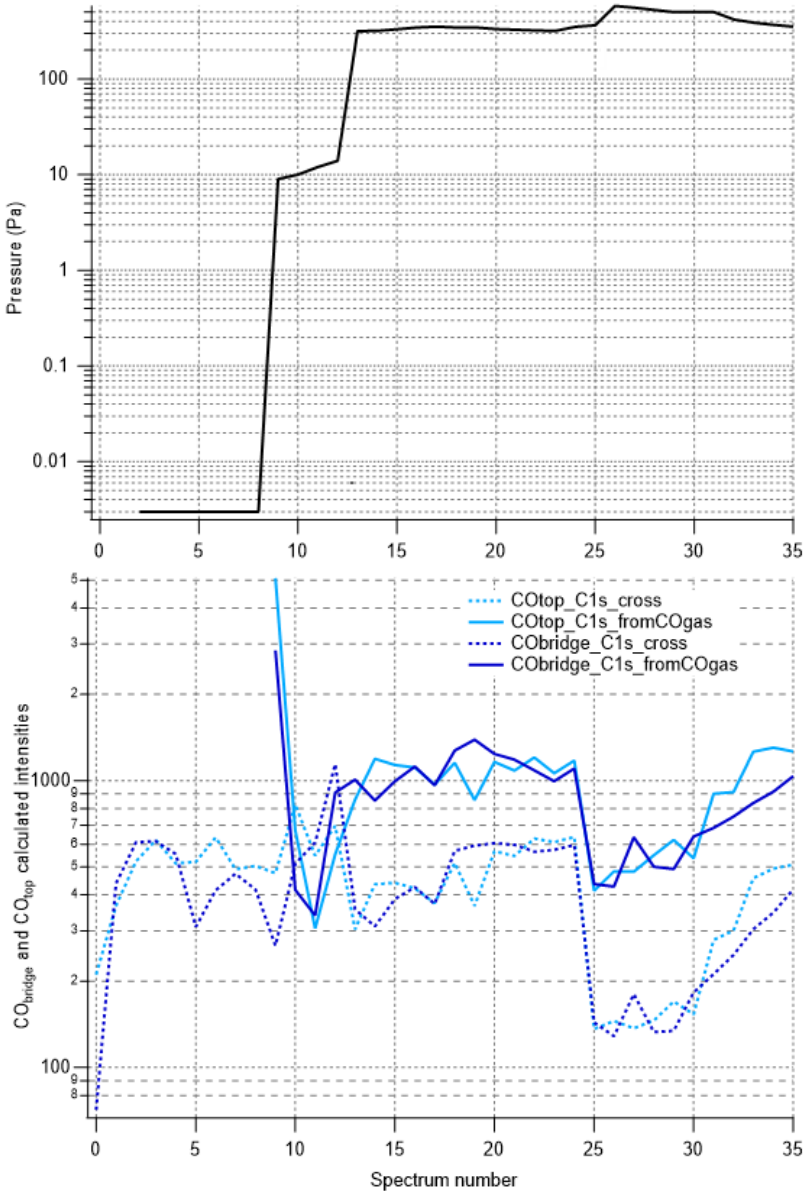

Figure 26 – a) CO pressure and b) adsorbed CO_{bridge} and CO_{top} intensities calculated according the two different assumptions described in the text: Intensity compared using the carbon and oxygen photoemission cross-section (dotted lines) and calculated according to equation 5 of chapter 3.2 (continuous lines).

In Fig. 27 I show the evolution of the spectra recorded sequentially while increasing the chamber pressure. At 0.1 mbar, in O 1s region, I observe an increase of the adsorbed CO species (532.2 eV and 531.0 eV). Also, I observe a little amount of dissociated oxygen (529.5 eV) and the unattributed specie at 526.7 eV present also initially before CO exposure. No significant change occurs in C 1s region.

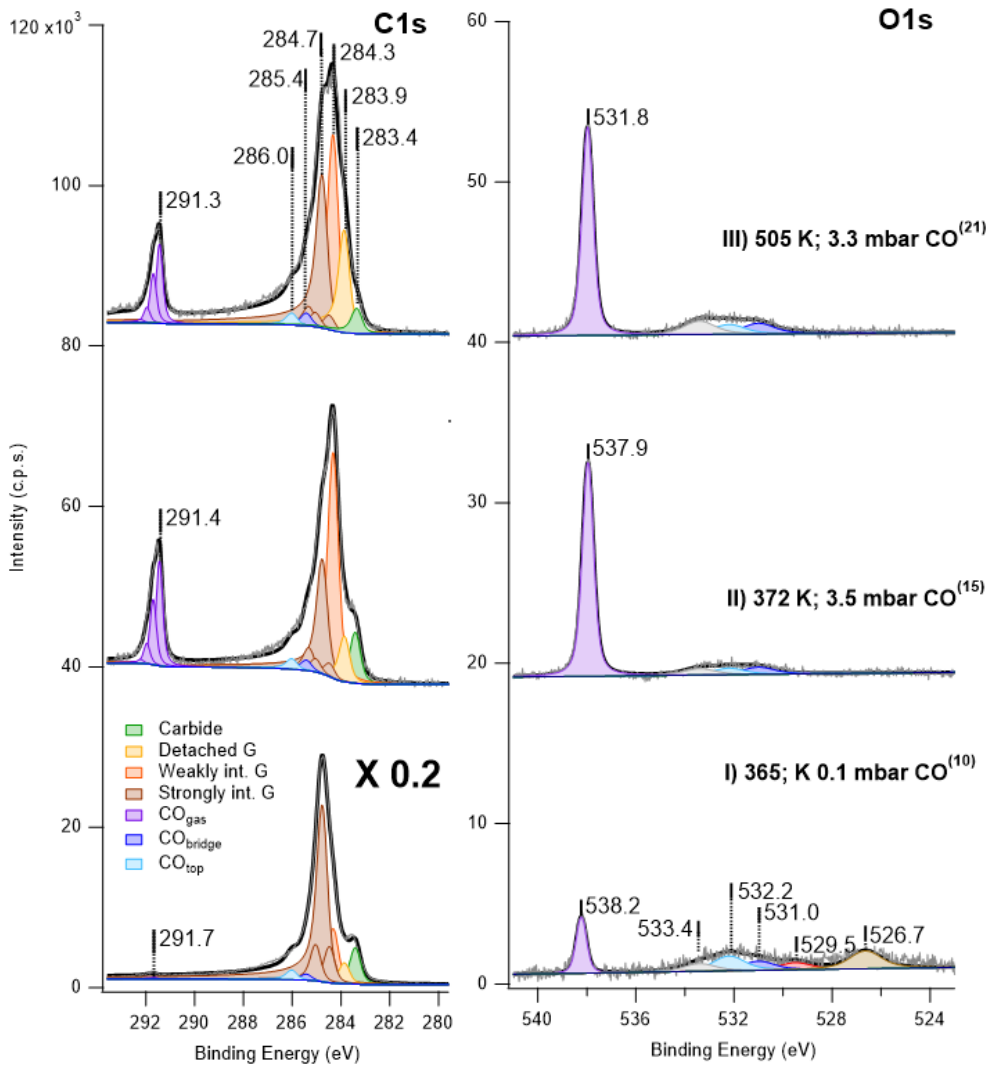

Figure 27 – NAP-XPS spectra of the C1s (left) and O1s (right) regions for G/Ni(111) : I) after sputtering at 365 K and in 0.1 mbar CO; II) 372 K and in 3.5 mbar CO; III) 505 K and in 3.3 mbar CO. As recorded spectra are shown without normalization.

At 3.5 mbar and 413 K, in the O 1s region, the impurity signal at 526.7 eV and the dissociated oxygen feature have disappeared and a component at 533.4 eV grows. This peak cannot be assigned to physisorbed CO_2 as in the previous experiments since it is not accompanied by its companion in the carbon region. A Different explanation has therefore to be found.

I notice that in the C 1s region the corresponding spectra show the transformation of more than half of the strongly interacting graphene signal into weakly and detached graphene. This observation implies that intercalation of CO has taken place. Despite not being clearly visible from the spectra due to the change of pressure, from the analysis of Fig. 20 an increase of the adsorbed CO coverage is clearly noticeable, regardless of the assumptions made in the analysis.

Upon increasing the temperature to 500 K the shape and the calculated coverages in the oxygen region remain constant while in C 1s region I observe a partial transformation of weakly interacting graphene into detached graphene.

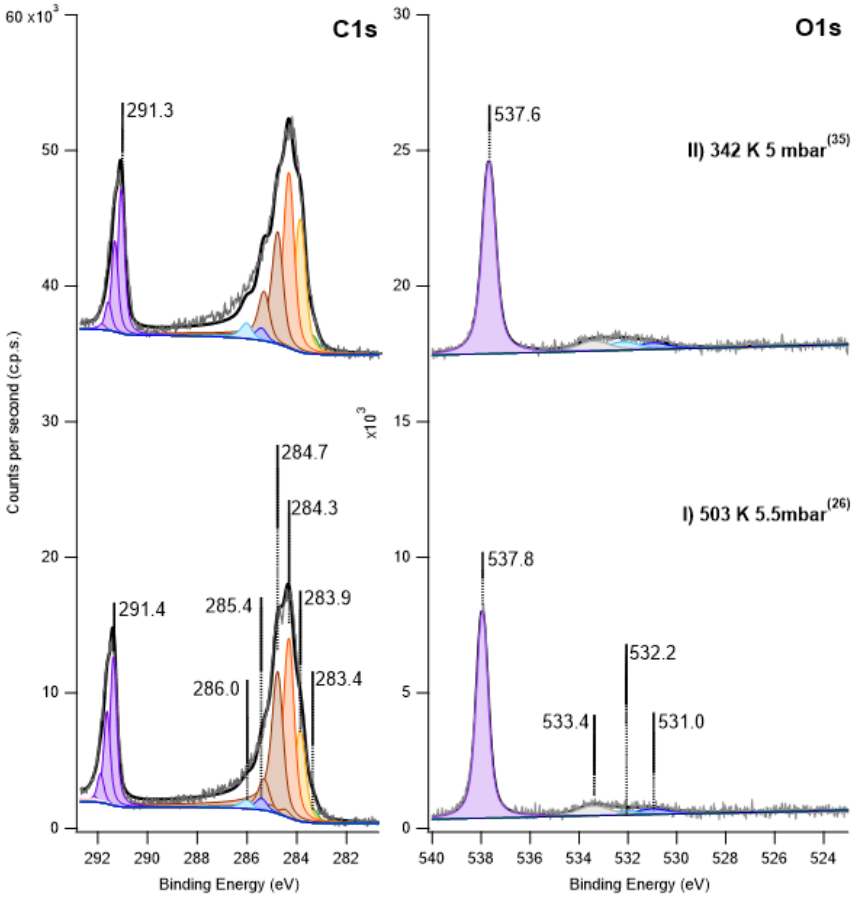

Figure 28 – NAP-XPS spectra of the C1s (left) and O1s (right) regions for sputtered G/Ni(111) : I) 500 K and 3.5 mbar CO; II) 500 K and 5.5 mbar CO; III) 400 K and 5.5 mbar CO; III) 350 K and 5.0 mbar CO. Spectra have not been normalized.

Upon increasing the CO pressure up to 5.0 mbar at 500 K (Fig. 28 I) no significant changes are observed in the carbon peak shape and in the coverages calculated from the O 1s intensities. Finally, in Fig. 28 II the spectra recorded after cooling down the system at 5.0 mbar are reported. Here, I observe an increase of the graphene intensity in the region between 286.0 eV and 289.0 eV.
This effect is due in part to a signal present also after CO removal (as discussed later) but could also be related to an increase of the graphene peak asymmetry, already noticed in the experiment described in the previous chapter upon the cooling down of the system in mbar CO pressure. Furthermore, in both experiments I observe an excess of CO_{top} intensity that witnesses the presence of weakly chemisorbed CO on graphene.

To analyze the evolution of the spectra, I report a synoptic figure with the coverage of the main species together with the temperature and the pressure during the experimental run as a function of the spectra number.

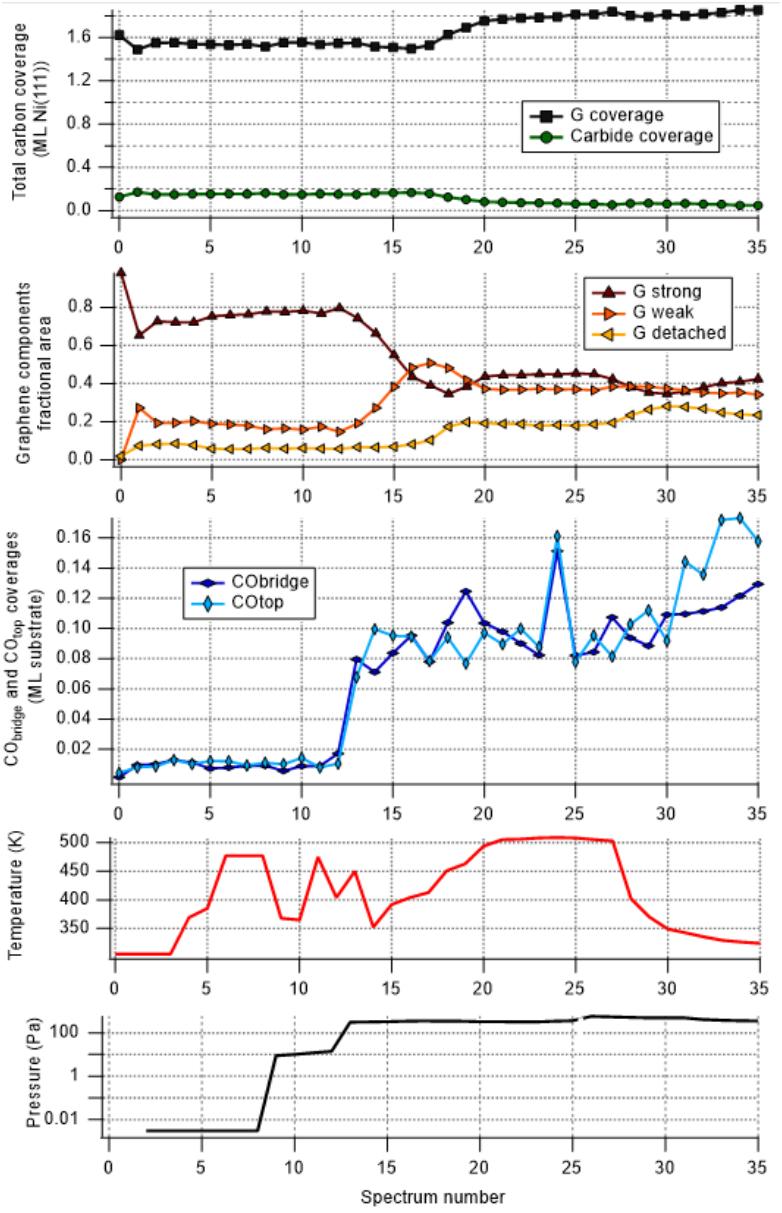

Figure 29 - a) Carbon coverages of graphene (black) and carbide (green); b) Fractional areas of the different graphene components (strongly interacting (brown); weakly interacting (mustard); detached (light-blue) and total (black)), and of nickel carbide (green) vs spectrum number; c) CO top and CO bridge coverages; d) Sample temperature; e) Sample pressure.

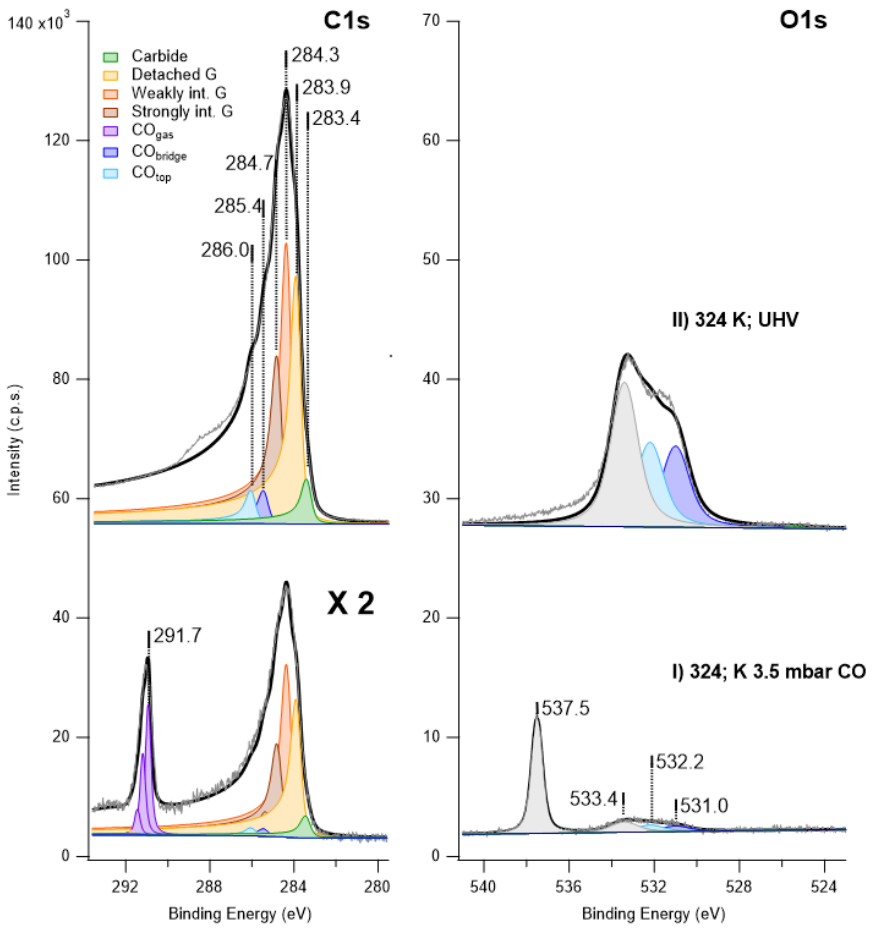

Figure 30 – spectra of the C1s (left) and O1s (right): I) 324 K and 3.5 mbar CO; II) immediately after CO NAP removal 324 K and UHV.

While the previous part of the experiment is similar to what observed for CO exposure on pristine graphene, in the present experiment on the sputtered graphene layer I observe a completely different behavior upon CO removal: contrary to the previous experiment the detached graphene component as well as the intensity at 533.4 eV persist after evacuation. The latter observation is also at odds with an assignment to physisorbed CO_2. After removal of the CO partial pressure a shoulder between 286.0 eV and 289 eV becomes evident. An asymmetry is now present also in the O 1s peak shape.

A possible explanation for these phenomena is the following: the absence of physisorbed CO_2, implies that this species is either not created or removed by reaction with the vacancies in the graphene layer created by the sputtering procedure. CO_2 could react to produce covalently bonded carbonaceous species which fill up the vacancy ending up in a bridge configuration over the holes. This interpretation is supported by the intensity of the carbon peak tail, particularly evident after evacuation, that, together with the feature at 533.4 eV in O 1s region witnesses the presence of carboxyl or epoxy groups. Such groups change the doping of the graphene layer and thus the

intensity of the inelastic tail of the graphene peaks. The damaged graphene could, moreover, not be able to convert back to the strongly interacting phase due to the presence of such covalently bonded groups. Indeed, scars were observed by STM inspection after CO dosing of the defected graphene layer (Celasco 2016). This mending of the holes would explanain also the decreased sticking probability for CO reported by HREELS inspection for subsequent additional CO exposures (Smerieri 2015).

Alternatively, the feature at 533.4 eV and the graphene tail could be related to the interaction of the system with a highly reactive species produced by the photolysis of the gas molecules in the NAP regime. This phenomenon has been extensively reported in literature but can hardly explain all our experimental picture.

I conclude, therefore, that the holes drilled in the graphene layer (and/or the damaged Ni surface below it) are likely to favor the transformation of CO_2 into strongly bonded species placed in bridge configuration across the holes and filling them up.

7. Conclusions

In my work I studied the reactivity of Ni(111) partially covered by carbide island with respect CO under near ambient pressure and, with in-operando XPS experiments I showed that graphene forms when dosing Ni(111) with CO already at 550 K, i.e. at a temperature significantly lower than the one required when hydrocarbons are used as precursors. The relevant catalytic process is most probably the Boudouard reaction. The latter implies CO_2 formation which we observe indeed by XPS after the graphene layer has formed, i.e. in conditions when it can accumulate below it. For reaction temperatures 600 K < T < 720 K the reactants must consist of intercalated CO and the disproportionation reaction must take place "under cover" to permit the so-produced physisorbed CO_2 to accumulate in a sufficient amount to be detected by XPS.

These results contribute to the general understanding of processes that occur at nickel surfaces and graphene/nickel interfaces at elevated CO pressures, in particular of Ni-catalyzed chemical reactions occurring under a 2D cover.

I also have investigated CO intercalation underneath G on Ni(111) under so far unexplored in-operando NAP conditions. My experiments show that:

a) CO intercalates below graphene binding to Ni(111) both at atop and bridge sites, a condition indicating a local coverage of CO higher than the ones observed so far without monitoring the surface in real time.

b) This high local CO coverage enables formation of physisorbed CO_2 under the graphene cover via the Boudouard reaction already at 340 K. Its accumulation underneath graphene is evident in the NAP-XPS spectra, while the absence of the corresponding gas-phase signal indicates a small reaction probability. The generated carbon converts carbide into graphene enlarging the fraction of the graphene-covered surface. To the best of our knowledge, this results is the first demonstration of the occurrence of the Boudouard reaction on Ni(111) under a graphene cover. Since the reaction rate increases with CO pressure, we expect this result to be relevant under catalytic conditions on nickel-based catalysts involving the presence of gas-phase CO, also as a side product.

c) CO adsorbs above strongly interacting domains of the G layer, confirming our previous finding obtained in UHV at low temperature by high resolution electron energy loss spectroscopy (Smerieri 2015) and the prediction of the existence of a relevant equilibrium coverage of CO at RT in the mbar pressure range. Such weakly bound CO might effectively enable a higher rate for reactions involving CO thanks to the lower activation barrier.

These findings are expected to have an impact on the study of chemical reactions under cover (Santiso 2007) and contribute to filling the pressure gap between previous NAP studies and the real catalytic conditions at even higher pressures. Eventually, I carried a similar in-operando XPS

experiment on a graphene in which holes have been create through sputtering procedure. I these conditions, CO_2 is likely to react with the graphene vacancies, forming strongly bounded groups between the graphene and the Nickel layer. This work leaves space for future experiments to deepen the knowledge of the system. To further confirm the production of CO_2 it would be particularly appropriate to check its presence in the gas phase with a Quadrupole Mass Spectrometer (QMS). This measurement was expected to be performed during the beamtime but it was not possible due to a malfunction of the experimental apparatus. Another suitable technique that could further confirm my result and deliver additional information is Infrared Absorption Spectroscopy (IRAS). Such technique is in fact able to determine the species formed in the experiments and, in particular, could give reliable information on the species that form upon CO NAP exposure on sputtered graphene. Finally A Low Energy Electron Diffraction (LEED) and/or Scanning Tunneling Microscopy analysis would be valuable to provide structural information on the modifications of the G/Ni(111) system under CO pressure.

8. Bibliography

Achilli, S., S. Tognolini, E. Fava, S. Ponzoni, G. Drera, C. Cepek, L. L. Patera, C. Africh, E. Del Castillo, M. I. Trioni, and S. Pagliara. 2018. "Surface States Characterization in the Strongly Interacting Graphene/Ni(111) System." *New Journal of Physics* 20(10).

Africh, Cristina, Cinzia Cepek, Laerte L. Patera, Giovanni Zamborlini, Pietro Genoni, Tevfik O. Mentes, Alessandro Sala, Andrea Locatelli, and Giovanni Comelli. 2016. "Switchable Graphene-Substrate Coupling through Formation/Dissolution of an Intercalated Ni-Carbide Layer." *Scientific Reports* 6(January):1–8.

Africh, Cristina, Cinzia Cepek, Laerte L Patera, Giovanni Zamborlini, Pietro Genoni, Tevfik O. Menteş, Alessandro Sala, Andrea Locatelli, and Giovanni Comelli. 2016. "Switchable Graphene-Substrate Coupling through Formation / Dissolution of an Intercalated Ni-Carbide Layer." *Nature Publishing Group* (September 2015):1–8.

Avval, Tahereh G., Shiladitya Chatterjee, Stephan Bahr, Paul Dietrich, Michael Meyer, Andreas Thißen, and Matthew R. Linford. 2019. "Carbon Dioxide Gas, CO2(g), by near-Ambient Pressure XPS." *Surface Science Spectra* 26(1):014022.

Bandara, Athula, Satoshi Katano, Jun Kubota, Ken Onda, Akihide Wada, Kazunari Domen, and Chiaki Hirose. 1998. "The Effect of Co-Adsorption of on-Top CO on the Sum-Frequency Generation Signal of Bridge CO on the Ni(111) Surface." *Chemical Physics Letters* 290(1–3):261–67.

Blaylock, D. Wayne, Teppei Ogura, William H. Green, and Gregory J. O. Beran. 2009. "Computational Investigation of Thermochemistry and Kinetics of Steam Methane Reforming on Ni (111) under Realistic Conditions." (111):4898–4908.

Blomberg, S., M. J. Hoffmann, J. Gustafson, N. M. Martin, V. R. Fernandes, A. Borg, Z. Liu, R. Chang, S. Matera, K. Reuter, and E. Lundgren. 2013. "In Situ X-Ray Photoelectron Spectroscopy of Model Catalysts: At the Edge of the Gap." *Physical Review Letters* 110(11):1–5.

Bluhm, Hendrik, Michael Hävecker, Axel Knop-Gericke, Evgueni Kleimenov, Robert Schlögl, Detre Teschner, Valerii I. Bukhtiyarov, D. Frank Ogletree, and Mlquel Salmeron. 2004. "Methanol Oxidation on a Copper Catalyst Investigated Using in Situ X-Ray Photoelectron

Spectroscopy." *Journal of Physical Chemistry B* 108(38):14340–47.

Blume, Raoul, Dirk Rosenthal, Jean Philippe Tessonnier, Henan Li, Axel Knop-Gericke, and Robert Schlögl. 2015. "Characterizing Graphitic Carbon with X-Ray Photoelectron Spectroscopy: A Step-by-Step Approach." *ChemCatChem* 7(18):2871–81.

Bost, N., A. Canizarès, M. R. Ammar, N. Raimboux, P. Melin, P. Simon, and J. Poirier. 2016. "Probing the Structural Organisation of Sp 2 Carbons Obtained by the Boudouard Reaction Using in Situ Raman Scattering in Reducing Conditions." *Vibrational Spectroscopy*.

Celasco, E., G. Carraro, M. Smerieri, L. Savio, M. Rocca, and L. Vattuone. 2017. "Influence of Growing Conditions on the Reactivity of Ni Supported Graphene towards CO." *Journal of Chemical Physics* 146(10).

Chen, P., H. Zhang, G. Lin, Q. Hong, and K. R. Tsm. 1997. "Growth of Carbon Nanotubes By Catalytic Decomposition of CH or CO on Ni-MgO Catalyst?" 6223(10):1495–1501.

Chen, Yuan, Dragos Ciuparu, Sangyun Lim, Gary L. Haller, and Lisa D. Pfefferle. 2006. "The Effect of the Cobalt Loading on the Growth of Single Wall Carbon Nanotubes by CO Disproportionation on Co-MCM-41 Catalysts." 44:67–78.

Company, North-holland Publishing, X-ray Induced Effects, and During The. 1981. "Science 104 (1981)." *Nature* 104:199–203.

Crumlin, Ethan J., Hendrik Bluhm, and Zhi Liu. 2013. "In Situ Investigation of Electrochemical Devices Using Ambient Pressure Photoelectron Spectroscopy." *Journal of Electron Spectroscopy and Related Phenomena* 190(PART A):84–92.

Dahal, Arjun and Matthias Batzill. 2014a. "Graphene-Nickel Interfaces: A Review." *Nanoscale* 6(5):2548–62.

Dahal, Arjun and Matthias Batzill. 2014b. "Graphene–Nickel Interfaces: A Review." *Nanoscale* 6(5):2548.

Davì, R., G. Carraro, M. Stojkovska, M. Smerieri, L. Savio, M. Lewandowski, J. J. Gallet, F. Bournel, M. Rocca, and L. Vattuone. 2021. "Graphene Growth on Ni (1 1 1) by CO Exposure at near Ambient Pressure." *Chemical Physics Letters* 774(March):138596.

Dedkov, Yuriy and Elena Voloshina. 2015. "Graphene Growth and Properties on Metal Substrates." *Journal of Physics Condensed Matter* 27(30).

Ding, X., L. De Rogatis, E. Vesselli, A. Baraldi, G. Comelli, R. Rosei, L. Savio, L. Vattuone, M. Rocca, P. Fornasiero, F. Ancilotto, A. Baldereschi, and M. Peressi. 2007. "Interaction of Carbon Dioxide with Ni(110): A Combined Experimental and Theoretical Study." *Physical Review B* -

Condensed Matter and Materials Physics 76(19):1–12.

Dong, Aiyi, Qiang Fu, Mingming Wei, and Xinhe Bao. 2017. “Graphene-Metal Interaction and Its Effect on the Interface Stability under Ambient Conditions.” *Applied Surface Science*.

Fei, Xiangmin, Lizhi Zhang, Wende Xiao, Hui Chen, Liwei Liu, Kai Yang, Shixuan Du, Hong-jun Gao, and Just Accepted. 2015. “Structural and Electronic Properties of Pb- Intercalated Graphene on Ru (0001) Structural and Electronic Properties of Pb- Intercalated Graphene on Ru (0001).” (0001).

Fu, Qiang and Xinhe Bao. 2017. “Surface Chemistry and Catalysis Confined under Two-Dimensional Materials.” *Chemical Society Reviews* 46(7):1842–74.

Gao, Lijun, Qiang Fu, Jiamin Li, Zhenping Qu, and Xinhe Bao. 2016. “Enhanced CO Oxidation Reaction over Pt Nanoparticles Covered with Ultrathin Graphitic Layers.” *Carbon* 101:324–30.

Gao, Lijun, Qiang Fu, Mingming Wei, Yifeng Zhu, Qiang Liu, Ethan Crumlin, Zhi Liu, and Xinhe Bao. 2016. “Enhanced Nickel Catalyzed Methanation Confined under Hexagonal Boron Nitride Shells Enhanced Nickel Catalyzed Methanation Confined under Hexagonal Boron Nitride Shells.”

Giovannetti, G., P. A. Khomyakov, G. Brocks, V. M. Karpan, J. Van Den Brink, and P. J. Kelly. 2008. “Doping Graphene with Metal Contacts.” *Physical Review Letters* 101(2):4–7.

Gyamfi, M., T. Eelbo, M. Wa, and R. Wiesendanger. 2011. “Inhomogeneous Electronic Properties of Monolayer Graphene on Ru (0001) MLg.” 153418:1–4.

Hammer, B. and K. Norskov. 1997. “CO Adsorption and Dissociation on Pt (111) and Ni(111) Surfaces.” 386:67–72.

Han, Young Kyu, Chang-il Ahn, Jong-wook Bae, A. Rong Kim, and Gui Young Han. 2013. “E Ff Ects of Carbon Formation on Catalytic Performance for CO 2 Reforming with Methane on Ni / Al 2 O 3 Catalyst : Comparison of Fixed- Bed with Fluidized-Bed Reactors.” 13288(1).

Heintz, J. .., F. Weill, and J. .. Bernier. 1989. “Characterization of Agglomerates by Ceramic Powder Compaction.” *Materials Science and Engineering: A* 109:271–77.

Held, G., J. Schuler, W. Sklarek, and H. P. Steinrück. 1998. “Determination of Adsorption Sites of Pure and Coadsorbed CO on Ni(111) by High Resolution X-Ray Photoelectron Spectroscopy.” *Surface Science* 398(1–2):154–71.

Hunt, Jacob, Anthony Ferrari, Adrian Lita, Mark Crosswhite, Bridgett Ashley, and A. E. Stiegman. 2013. “Microwave-Speci Fi c Enhancement of the Carbon − Carbon Dioxide (Boudouard)

Reaction."

Itikawa, Yukikazu. 2002. "Cross Sections for Electron Collisions with Carbon Dioxide." *Journal of Physical and Chemical Reference Data* 31(3):749–67.

Jacobson, Peter, Bernhard Stöger, Andreas Garhofer, Gareth S. Parkinson, Michael Schmid, Roman Caudillo, Florian Mittendorfer, Josef Redinger, and Ulrike Diebold. 2012. "Nickel Carbide as a Source of Grain Rotation in Epitaxial Graphene." *ACS Nano* 6(4):3564–72.

Jorio, Ado. 2012. "Raman Spectroscopy in Graphene-Based Systems: Prototypes for Nanoscience and Nanometrology." *ISRN Nanotechnology* 2012:1–16.

Kahk, J. Matthias and Johannes Lischner. 2018. "Core Electron Binding Energies of Adsorbates on Cu(111) from First-Principles Calculations." *Physical Chemistry Chemical Physics* 20(48):30403–11.

Kamath, P. Vishnu and C. N. R. Rao. 1984. "Electron Spectroscopic Studies of Oxygen and Carbon Dioxide Adsorbed on Metal Surfaces." *Journal of Physical Chemistry* 88(3):464–69.

Knop-Gericke, Axel, Evgueni Kleimenov, Michael Hävecker, Raoul Blume, Detre Teschner, Spiros Zafeiratos, Robert Schlögl, Valerii I. Bukhtiyarov, Vasily V. Kaichev, Igor P. Prosvirin, Alexander I. Nizovskii, Hendrik Bluhm, Alexei Barinov, Pavel Dudin, and Maya Kiskinova. 2009. *Chapter 4 X-Ray Photoelectron Spectroscopy for Investigation of Heterogeneous Catalytic Processes*. Vol. 52. 1st ed. Elsevier Inc.

Lahiri, Jayeeta, Travis Miller, Lyudmyla Adamska, Ivan I. Oleynik, and Matthias Batzill. 2011. "Graphene Growth on Ni(111) by Transformation of a Surface Carbide." *Nano Letters* 11(2):518–22.

Lehtinen, O., J. Kotakoski, A. V. Krasheninnikov, A. Tolvanen, K. Nordlund, and J. Keinonen. 2010. "Effects of Ion Bombardment on a Two-Dimensional Target: Atomistic Simulations of Graphene Irradiation." *Physical Review B - Condensed Matter and Materials Physics* 81(15):1–4.

Li, Yanwu, Yongjun Cheng, Wenjun Sun, Yongjun Wang, Meng Dong, and Lian Chen. 2017. "Study of Physisorption Isotherm of Water on Technical Nickel Surface with a Wide Pressure Range." *Vacuum* 145:123–27.

Liu, Hang, Alter Zakhtser, Ahmed Naitabdi, François Rochet, Fabrice Bournel, Caroline Salzemann, Christophe Petit, Jean Jacques Gallet, and Wanqi Jie. 2019. "Operando Near-Ambient Pressure X-Ray Photoelectron Spectroscopy Study of the CO Oxidation Reaction on the Oxide/Metal Model Catalyst ZnO/Pt(111)." *ACS Catalysis* 9(11):10212–25.

Liu, Nan, Lei Fu, Boya Dai, Kai Yan, Xun Liu, Ruiqi Zhao, Yanfeng Zhang, and Zhongfan Liu. 2011. "Universal Segregation Growth Approach to Wafer-Size Graphene from Non-Noble Metals." *Nano Letters* 11(1):297–303.

Monachino, Enrico, Mark Greiner, Axel Knop-Gericke, Robert Schlögl, Carlo Dri, Erik Vesselli, and Giovanni Comelli. 2014. "Reactivity of Carbon Dioxide on Nickel: Role of CO in the Competing Interplay between Oxygen and Graphene." *Journal of Physical Chemistry Letters* 5(11):1929–34.

Nakano, H., S. Kawakami, T. Fujitani, and J. Nakamura. 2000. "Carbon Deposition by Disproportionation of CO on a Ni (977) Surface." 456:295–99.

Ni, O. N., C. Astaldi, A. Santoni, F. Della Valle, and R. Rose. 1989. "Ni(100) C. ASTALDI ', A. SANTONI 234, F. DELLA VALLE 133 and R. ROSE1 334 ."" 220:322–32.

Novoselov, K. S., A. K. Geim, S. V. Morozov, D. Jiang, M. I. Katsnelson, I. V. Grigorieva, S. V. Dubonos, and A. A. Firsov. 2005. "Two-Dimensional Gas of Massless Dirac Fermions in Graphene." *Nature* 438(7065):197–200.

Ogletree, D. Frank, Hendrik Bluhm, Gennadi Lebedev, Charles S. Fadley, Zahid Hussain, and Miquel Salmeron. 2002. "A Differentially Pumped Electrostatic Lens System for Photoemission Studies in the Millibar Range." *Review of Scientific Instruments* 73(11):3872.

Panagiotopoulou, Paraskevi, Dimitris I. Kondarides, and Xenophon E. Verykios. 2011. "Mechanistic Study of the Selective Methanation of CO over Ru / TiO 2 Catalyst : Identification of Active Surface Species and Reaction Pathways †." 1220–30.

Papaefthimiou, V., T. Dintzer, M. Lebedeva, D. Teschner, M. Hävecker, A. Knop-Gericke, R. Schlögl, V. Pierron-Bohnes, E. Savinova, and S. Zafeiratos. 2012. "Probing Metal-Support Interaction in Reactive Environments: An in Situ Study of PtCo Bimetallic Nanoparticles Supported on TiO 2." *Journal of Physical Chemistry C* 116(27):14342–49.

Patel, Dhananjay I., Dhruv Shah, Stephan Bahr, Paul Dietrich, Michael Meyer, Andreas Thißen, and Matthew R. Linford. 2019. "Water Vapor, by near-Ambient Pressure XPS." *Surface Science Spectra* 26(1):014026.

Patera, Laerte L., Cristina Africh, Robert S. Weatherup, Raoul Blume, Sunil Bhardwaj, Carla Castellarin-Cudia, Axel Knop-Gericke, Robert Schloegl, Giovanni Comelli, Stephan Hofmann, and Cinzia Cepek. 2013. "In Situ Observations of the Atomistic Mechanisms of Ni Catalyzed Low Temperature Graphene Growth." *ACS Nano* 7(9):7901–12.

Pavelec, Jiri, Jan Hulva, Daniel Halwidl, Roland Bliem, Oscar Gamba, Zdenek Jakub, Florian

Brunbauer, Michael Schmid, Ulrike Diebold, and Gareth S. Parkinson. 2017. “A Multi-Technique Study of CO2 Adsorption on Fe3O4 Magnetite.” *Journal of Chemical Physics* 146(1).

Peng, Guowen, Lindsay R. Merte, Jan Knudsen, Ronnie T. Vang, Erik Lægsgaard, Flemming Besenbacher, and Manos Mavrikakis. 2010. “On the Mechanism of Low-Temperature CO Oxidation on Ni(111) and NiO(111) Surfaces.” *Journal of Physical Chemistry C* 114(49):21579–84.

Perilli, Daniele, Sara Fiori, Mirco Panighel, Hongsheng Liu, Cinzia Cepek, Maria Peressi, Giovanni Comelli, Cristina Africh, and Cristiana Di Valentin. 2020. “Mechanism of CO Intercalation through the Graphene/Ni(111) Interface and Effect of Doping.” *Journal of Physical Chemistry Letters* 11(20):8887–92.

Del Puppo, Simone, Virginia Carnevali, Daniele Perilli, Francesca Zarabara, Alberto Lodi Rizzini, Gabriele Fornasier, Erik Zupanič, Sara Fiori, Laerte L. Patera, Mirco Panighel, Sunil Bhardwaj, Zhiyu Zou, Giovanni Comelli, Cristina Africh, Cinzia Cepek, Cristiana Di Valentin, and Maria Peressi. 2021. “Tuning Graphene Doping by Carbon Monoxide Intercalation at the Ni(111) Interface.” *Carbon* 176:253–61.

Roiaz, Matteo, Enrico Monachino, Carlo Dri, Mark Greiner, Robert Schloegl, Giovanni Comelli, and Erik Vesselli. 2016. “Reverse Water-Gas Shift or Sabatier Methanation on Ni (110)? Stable Surface Species at near-Ambient Pressure.” (110).

Rosei, R., F. Ciccacci, R. Memeo, C. Mariani, L. S. Caputi, and L. Papagno. 1983. “Kinetics of Carbidic Carbon Formation from CO in the 10-6-Torr Range on Ni (Ll0).” 24:19–24.

Santiso, Erik E., Milen K. Kostov, Aaron M. George, Marco Buongiorno Nardelli, and Keith E. Gubbins. 2007. “Confinement Effects on Chemical Reactions-Toward an Integrated Rational Catalyst Design.” *Applied Surface Science* 253(13 SPEC. ISS.):5570–79.

Schnadt, Joachim, Jan Knudsen, Jesper N. Andersen, Hans Siegbahn, Annette Pietzsch, Franz Hennies, Niclas Johansson, Nils Mårtensson, Gunnar Öhrwall, Stephan Bahr, Sven Mähl, and Oliver Schaff. 2012. “The New Ambient-Pressure X-Ray Photoelectron Spectroscopy Instrument at MAX-Lab.” *Journal of Synchrotron Radiation* 19(5):701–4.

Shavorskiy, Andrey, Osman Karslioglu, Ioannis Zegkinoglou, and Hendrik Bluhm. 2014. “Synchrotron-Based Ambient Pressure X-Ray Photoelectron Spectroscopy.” *Synchrotron Radiation News* 27(2):14–23.

Siegbahn, Hans. 1985. “Electron Spectroscopy for Chemical Analysis of Liquids and Solutions.”

Journal of Physical Chemistry 89(6):897–909.

Siegbahn, Hans and Kai Siegbahn. 1973. “ESCA Applied to Liquids.” *Journal of Electron Spectroscopy and Related Phenomena* 2(3):319–25.

Smerieri, Marco, Edvige Celasco, Giovanni Carraro, Angelique Lusuan, Jagriti Pal, Gianangelo Bracco, Mario Rocca, Letizia Savio, and Luca Vattuone. 2015. “Enhanced Chemical Reactivity of Pristine Graphene Interacting Strongly with a Substrate: Chemisorbed Carbon Monoxide on Graphene/Nickel(1 1 1).” *ChemCatChem* 7(15):2328–31.

Snoeck, J. and G. F. Froment. 2002. “Steam / CO 2 Reforming of Methane . Carbon Filament Formation by the Boudouard Reaction and Gasification by CO 2 , by H 2 , and by Steam : Kinetic Study.” 4252–65.

Stuckless, J. T., N. Al-Sarraf, C. Wartnaby, and D. A. King. 1993. “Calorimetric Heats of Adsorption for CO on Nickel Single Crystal Surfaces.” *Journal of Chemical Physics* 99(3):2202–12.

Susi, Toma, Thomas Pichler, and Paola Ayala. 2015. “X-Ray Photoelectron Spectroscopy of Graphitic Carbon Nanomaterials Doped with Heteroatoms.” *Beilstein Journal of Nanotechnology* 6(1):177–92.

Trenary, M., K. J. Uram, and J. T. Yates. 1985. “An Infrared Reflection-Absorption Study of CO Chemisorbed on Clean and Sulfided Ni(111) - Evidence for Local Surface Interactions.” *Surface Science* 157(2–3):512–38.

Trotochaud, Lena, Ashley R. Head, Osman Karslioğlu, Line Kyhl, and Hendrik Bluhm. 2017. “Ambient Pressure Photoelectron Spectroscopy: Practical Considerations and Experimental Frontiers.” *Journal of Physics Condensed Matter* 29(5).

Ugeda, M. M., D. Fernández-Torre, I. Brihuega, P. Pou, A. J. Martínez-Galera, Rubén Pérez, and J. M. Gómez-Rodríguez. 2011. “Point Defects on Graphene on Metals.” *Physical Review Letters* 107(11):1–5.

Ugeda, Miguel M., Iván Brihuega, Fanny Hiebel, Pierre Mallet, Jean Yves Veuillen, José M. Gómez-Rodríguez, and Félix Ynduráin. 2012. “Electronic and Structural Characterization of Divacancies in Irradiated Graphene.” *Physical Review B - Condensed Matter and Materials Physics* 85(12):2–6.

Vesselli, Erik, Loredana De Rogatis, Xunlei Ding, Alessandro Baraldi, Letizia Savio, Luca Vattuone, Mario Rocca, Paolo Fornasiero, Maria Peressi, Alfonso Baldereschi, Renzo Rosei, and Giovanni Comelli. 2008. “Carbon Dioxide Hydrogenation on Ni(110).” *Journal of the American Chemical Society* 130(34):11417–22.

Weatherup, Robert S., Bernhard C. Bayer, Raoul Blume, Caterina Ducati, Carsten Baehtz, Robert Schlögl, and Stephan Hofmann. 2011. “In Situ Characterization of Alloy Catalysts for Low-Temperature Graphene Growth.” *Nano Letters* 11(10):4154–60.

Wei, Mingming, Qiang Fu, Yang Yang, Wei Wei, Ethan Crumlin, Hendrik Bluhm, and Xinhe Bao. 2015. “Modulation of Surface Chemistry of CO on Ni(111) by Surface Graphene and Carbidic Carbon.” *Journal of Physical Chemistry C* 119(24):13590–97.

Yao, Yunxi, Qiang Fu, Zhen Wang, Dali Tan, and Xinhe Bao. 2010. “Growth and Characterization of Two-Dimensional FeO Nanoislands Supported on Pt(111).” *Journal of Physical Chemistry C* 114(40):17069–79.

Yao, Yunxi, Qiang Fu, Y. Y. Zhang, Xuefei Weng, Huan Li, Mingshu Chen, Li Jin, Aiyi Dong, and Rentao Mu. 2014. “Graphene Cover-Promoted Metal-Catalyzed Reactions.” 111(48).

Yeh, J. J. and I. Lindau. 1985. “Copyright 0 1985 by Academic Press, Inc.” *Atomic Data and Nuclear Data Tables* 32(l):1–155.

Zhao, Wei, Sergey M. Kozlov, Oliver Höfert, Karin Gotterbarm, Michael P. A. Lorenz, Francesc Viñes, Christian Papp, Andreas Görling, and Hans Peter Steinrück. 2011. “Graphene on Ni(111): Coexistence of Different Surface Structures.” *Journal of Physical Chemistry Letters* 2(7):759–64.

Zou, Zhiyu, Lei Fu, Xiuju Song, Yanfeng Zhang, and Zhongfan Liu. 2014. “Carbide-Forming Groups IVB-VIB Metals: A New Territory in the Periodic Table for CVD Growth of Graphene.” *Nano Letters* 14(7):3832–39.